© Copyright 2020
Richard V. Lee

Heterofunctional Solid-Binding Peptides for Nucleic Acid Sensing Towards the Development of Cancer Biosensors

Richard V. Lee

A thesis submitted in partial fulfillment of the requirements for the degree of

Master of Science
in
Materials Science and Engineering

University of Washington

2020

Committee:

Mehmet Sarikaya

Devin MacKenzie

Sami Dogan

Program Authorized to Offer Degree:

Materials Science & Engineering

University of Washington

Abstract

Heterofunctional Solid-Binding Peptides for Nucleic Acid Sensing
Towards the Development of Cancer Biosensors

Richard V. Lee

Chair of the Supervisory Committee:
Mehmet Sarikaya
Department of Materials Science and Engineering

A key challenge in designing biosensors is achieving high detection sensitivity without compromising target specificity. Field-effect transistors based on 2D solids offer enhanced sensitivity due to their atomically thin characteristics. Still, such biosensors must possess several critical attributes to detect ultra-low target concentrations within a bodily fluid: 1) Probes must be securely immobilized onto the 2D-layer substrate; 2) Optimal molecular packing of the probe must be controlled for efficient target capture; 3) Non-specific adsorption of off-target molecules must be prevented; and 4) Non-covalent functionalization of the sensing surface is favored to avoid creating surface defects that could affect sensing properties. Achieving these attributes presents several major obstacles.

In the present research, these challenges are addressed to set the foundation for further development towards a versatile cancer diagnostic device. An anti-fouling graphene-binding peptide (GrBP) was used to confer passivating properties onto the sensing surface which mitigates non-specific protein adsorption, while a heterofunctional GrBP chimera bearing a peptide nucleic acid linker was used (GrBP-PNA) to immobilize DNA probes onto the sensing surface. Sensor surface functionalization, followed by subsequent target capture, was confirmed using surface plasmon resonance (SPR) and quartz crystal microbalance (QCM) analysis. Raman spectroscopy of the graphene FET device revealed a pristine

surface ready functionalization in order to detect nucleic acid biomarker targets. The results provide a viable biosensing strategy for versatile nucleic acid sensing using a modular probe design. This modular approach and anti-fouling method can allow for the eventual goal of collecting miRNA expression profiles from complex biological liquids for clinical diagnosis and prognosis of various diseases.

Table of Contents

1. Hypothesis

Graphene field-effect transistor (FET) biosensors functionalized with hybrid peptide-PNA constructs display improved device performance in the detection of nucleic acid biomarker targets.

2. Statement of the Problem

Biosensors show great promise for early detection and diagnosis of cancers, diseases, and other ailments. With the abundance of microRNA (miRNA) biomarkers comes a plethora of potential targets for facile diagnosis and monitoring of a wide range of diseases. However, the diagnostic power of miRNAs is limited by the ability to reliably detect these biomolecules in clinical settings. With the right device architecture and biosensing strategy, there is unlimited potential for diagnosing life-threatening disease and its intermittent monitoring.

A nanobiosensing platform that can non-invasively sense multiple miRNA species simultaneously, directly from complex biological fluids (such as saliva, urine, plasma or serum), with high selectivity and sensitivity, while sampling characteristic disease signatures from various pathologies can help transform modern healthcare. For example, implementing label-free, direct detection of nucleic acids within an array format as a routine screening tool for clinical annual checkups to survey a panel of miRNA biomarkers would help identify early and late stages of various cancers along with other ailments, such as cardiovascular and autoimmune diseases. Doing so could better discriminate pancreatic cancer from other cancers,[1,2] as well as from non-malignant abnormalities (e.g. chronic pancreatitis)[3-5] based on their differing miRNA signatures—leading to more effective and earlier diagnosis of potentially lethal maladies.

3. Introduction

Early detection of pancreatic cancer remains a current medical challenge, and presents an opportunity for developing effective tools for timely diagnosis. Pancreatic cancer is the only cancer with 5-year survival rates of less than 10% (only 2% for distant stages).[6] Roughly 53,000 new cases were

projected in 2016 in USA, with an estimated 41,780 deaths.[6] In 2012, pancreatic cancer was ranked fourth in cancer-related deaths[6] and is projected to rank second as early as 2020.[7] Early diagnosis remains a current challenge owing to the absence of symptoms that do not manifest until advanced stages of disease, while regular screening of asymptomatic patients is largely ineffective.[8] Late-stage detection results in poor prognosis since treatment options become limited and futile due to metastasis. Mean total direct medical costs ($65,500) reveal the heavy financial burden posed by this disease.[9] To address this long-standing malignancy, a nanobiosensor array for multiplexed detection of pre-lesion and early-stage microRNA cancer biomarkers is proposed.

Dysregulated miRNA biomarkers expressed early during disease provide suitable targets for cancer biosensors. Moreover, miRNA dysregulation has been shown to distinguish pancreatic cancer patients from healthy individuals via whole blood sampling.[10] miRNAs in plasma[11] and serum[3] have also been used for determining pancreatic ductal adenocarcinoma (PDAC), while early stage and Stage I PDAC miRNAs have been found in urine and used for microarray analysis.[5] Consequently, an opportunity arises for applying miRNA indices (i.e., expression profiles) to discern disease states from normal, healthy ones.

However, miRNA biosensing technology is not yet mature and to date no such clinical or commercial devices exist. Previous studies in this research group have proven the feasibility and application of a peptide-enabled graphene biosensor for detecting proteinaceous CA-19 and CEA cancer biomarkers. This research will build on the previously established principles of peptide-based modular assembly and sensor functionalization in order to create a highly sensitive nanobiosensor array for multiplexed detection of nucleic acid biomarker targets from healthy and disease-state samples of plasma, serum, saliva, and urine origin. If successful, then this research project will generate a platform technology for non-invasive detection, diagnosis, and prognosis of a variety of illnesses, disorders, and maladies.

This will be accomplished by using: (1) Novel solid-binding peptide-PNA chimeric constructs that confer modularity and versatility to biomarker detection and sensor functionalization; (2) Field-effect transistors based on two-dimensional materials that offer enhanced sensitivity due to their atomically thin

characteristics; and (3) Multiplexing array architectures that leverage the diagnostic power of miRNAs by cataloguing and comparing their abundance to map disease-specific signatures from disease onset to disease progression. The advantages conferred by each component (i.e., SBPs, PNAs, 2D materials) are proper probe display, sensor passivation against non-specific adsorption of biological interferants, and label-free nucleic acid detection independent from enzyme amplification. The unique modular design of the chimeric peptide-PNA constructs, FET biosensing approach, and application of nanostructure self-assembly principles allow for high sensitivity, acute specificity, and facile scalability towards a versatile sensor array for multiplexed miRNA expression profiling.

The project addresses the lack of cost-effective, point-of-care diagnosis for early cancer detection by exploiting the evolving abnormal miRNA profile expressed at various stages of disease in order to detect, identify, and characterize the type and stage of cancer. Although the deliverables include creating a nanobiosensor array for early diagnosis and prognosis of pancreatic cancer, the proposed sensing strategy can also be applied to other types of cancers and maladies by taking advantage of their own respective miRNA disease signatures.

4. Background

4.1. miRNA Biomarkers for Cancer Diagnosis and Monitoring

Biomarkers are biological molecules used to identify, characterize, or determine a biological state. These biomarkers can be of protein, nucleic acid, lipid, or other biological origin and are often quantified from biological samples, such as biopsies or blood. Typically, these molecules are released from cells or are byproducts of cellular processes, such as metabolites, thereby giving insight into the nature of disease and health. Their detectable presence can reveal clinically important information—for example, the degree of illness or how well a patient responds to treatments. Biomarkers can be diagnostic, prognostic, or staging types depending on when they are detectable during the disease process and their involvement in pathological functions.

Antibody assays are the most common type of biomarker diagnostic used in clinics. Although such protein-based assays are available for the detection of various ailments, nucleic acids are quickly becoming an important biomarker category, which includes microRNA (miRNA), circular RNA,[12-15] cell-free DNA,[16] and circulating tumor DNA.[17] Nucleic acid biomarkers therefore present an opportunity for diagnosis and prognosis of many illnesses and diseases by providing another avenue for detection and monitoring. Of particular interest are miRNAs which belong to a class of non-coding RNAs, and are distinct from messenger RNA (mRNA), the transcriptional template derived from DNA.

According to the central dogma of biology, permanent genetic information stored in DNA is transcribed into expendable messenger RNA (mRNA) for subsequent translation into amino acids that form proteins. Thus, expression of this genetic information (i.e., genotype) results in the physical attributes (i.e., phenotype) manifested by the organism. In contrast to messenger RNA, microRNAs are short nucleotide sequences (approximately 22 bases in length) and function primarily in regulating gene expression by inducing either mRNA degradation or translational repression[18] **(Fig. 1)**. The effect is gene silencing at the messenger RNA level. Because of their role in controlling protein levels and therefore the proteome landscape, miRNAs play a vital role in regulating cellular processes. Thus, dysregulation of microRNAs can therefore lead to abnormal gene expression causing detrimental effects on normal cellular functions.

Consequently, non-coding, circulating cell-free miRNAs[19,20] can provide a vast wealth of disease information[21] and have emerged as powerful indicators for a number of maladies: cancer,[22,23] viral infections,[24,25] cardiovascular disease,[26,27] and neurological disorders.[28-31] It has been revealed that miRNAs are implicated in a variety of cancers due to their various roles in cellular processes[32] **(Fig. 2)**. Importantly, specific miRNA species are known to play a role in the signaling pathways that give rise to pancreatic cancer—whereby their dysregulation leads to oncogenesis.[33,34] As such, miRNAs have been proposed as key therapeutic targets[35] for keeping cancers in check.[36] However, their true potential lies in their ability to foretell disease onset and progression.[37,38] Thus, there is great urgency in leveraging

miRNA expression profiles for early diagnosis of pancreatic cancer and identification of its disease stage.[39,40] The high stability of miRNAs in blood[41] and urine,[42] their detectable amounts in serum (5-290 fmol/L range),[3] and their ability to withstand repeated freeze-thaw cycles[43] allow for ready exploitation via robust biosensing.[44,45]

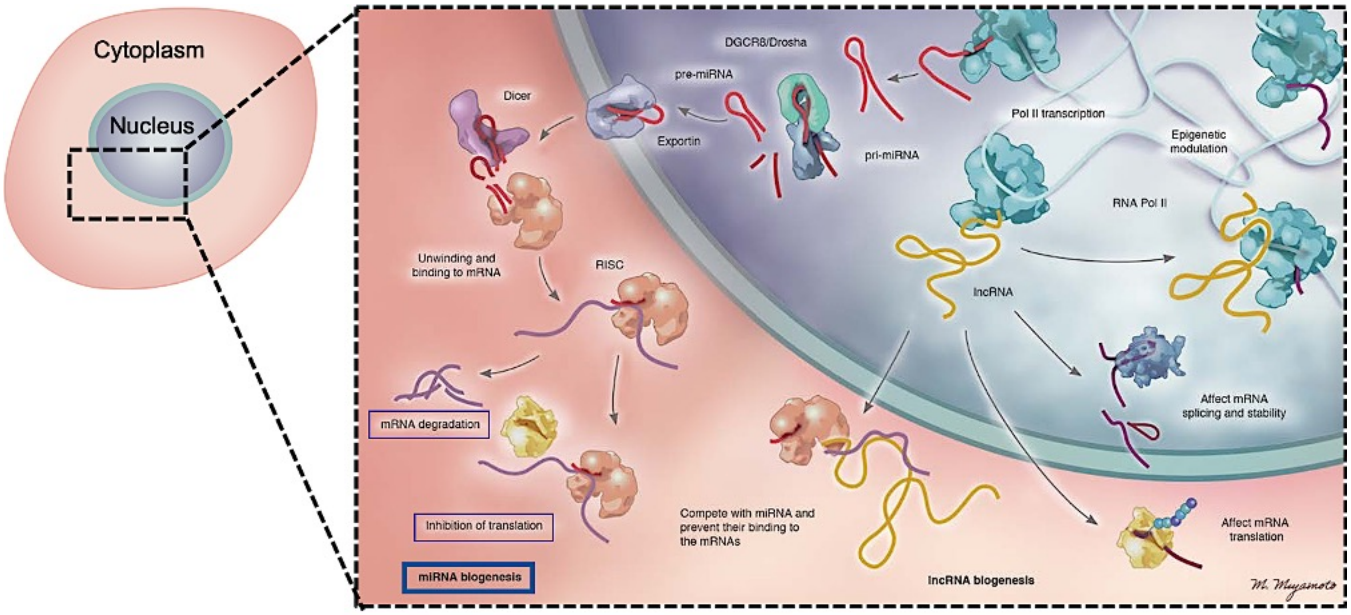

Figure 1. Schematic representation of miRNA intracellular function. Mature microRNA (miRNA) is exported from the nucleus and combines with the Dicer enzyme and a messenger RNA (mRNA) transcript to form the RNA-induced silencing complex (RISC). The mRNA is then degraded or is precluded from being translated into protein, resulting in gene silencing and the absence of protein expression. Modified from Vinny Negi et al. (2017).[18]

4.2. Field-Effect Transistor (FET)-based Biosensors

According to the International Union of Pure and Applied Chemistry (IUPAC) a biosensor is a device that uses specific biochemical reactions mediated by isolated enzymes, immunosystems, tissues, organelles or whole cells to detect chemical compounds, usually by electrical, thermal or optical signals.[46] A bionsensor consists of three main elements: (1) the analyte being sensed; (2) a biorecognition element anchored onto the sensing substrate that interacts with the analyte of interest; and (3) a transducer that senses the interaction between the biorecognition element and the analyte, which transforms that interaction into a signal that can be amplified, measured, and analyzed.

Important performance parameters include selectivity, sensitivity, lower limit of detection (LLD), and limit of quantification (LOQ). Selectivity is a measure of how well the sensor discriminates the analyte of interest from other analytes/molecules, whereas sensitivity is a measure of how well the sensor successfully measures the analyte of interest. It is important to note that these qualities refer specifically to *analytical* selectivity and sensitivity. In addition, there is also *clinical* sensitivity and *clinical* specificity—referring to the ability to correctly identify positive samples from negative samples (i.e., true positive rate), and distinguishing negative samples from positive samples (true negative rate), respectively.

Figure 2. Cancer-related miRNAs that control cellular processes. Various miRNA species play crucial roles in regulating cellular functions. Irregular expression of specific miRNAs can lead to abnormal gene upregulation or downregulation potentially causing tumorigenic behavior in cells and resultant oncological pathology. From Larrea et al. (2016).[32]

LLD is the smallest possible amount of analyte detectable by the biosensor and is defined as three standard deviations above the detectable background signal, while the LOQ is the smallest possible amount of analyte quantifiable and is defined as ten standard deviations above background.

Field-effect transistor (FET) biosensors are so named because their sensing mechanism is gated by the field-effect phenomenon whereby the conducting channel is set below a threshold potential that gets triggered by a biorecognition event to induce an electronic signal. Such biosensors have advanced in many areas—specifically, in the type of material used for the sensing channel (organic polymers, 2D materials), the device architecture (Bio-FET, solution gate), in addition to the already wide areas of sensing applications (e.g., gas detection). The advantage conferred by FET approaches to biosensing is the transduction of biological interactions into an electronic readout thereby creating a label-free approach to the sensing of molecules.

Recent advances[47] in biosensing technology have produced a variety of miRNA detection platforms[48] including electrochemical,[49] electromechanical,[50] and optical[51,52] approaches. However, FET biosensors[53-55] are sufficiently sensitive (fM to pM ranges) and forego sample preparation procedures, amplification and labeling steps—allowing a path for simple, cost-effective point-of-care diagnostics. Employing 2D materials (*e.g.,* graphene, MoS_2) can offer enhanced sensitivity due to their atomically thin (1<nm) characteristics whereby adsorption to its surface perturbs the electronic structure—resultantly providing the basis for detecting small amounts of analyte. Conversely, FET biosensors based on bulk 3D structures are limited by lower sensitivity. Similarly, although 1D structures such as nanowires or single-walled nanotubes (SWNTs) offer improved sensitivities, they are hampered by inconsistent production (e.g. purity, thickness, defects, chirality) resulting in variable device performance.[56]

Tunability of their electronic properties through chemical modification, doping or hybridization makes 2D materials ideal for biosensing applications. Advantages offered are their large surface areas that provide greater molecule adsorption compared to 1D structures, while their one-atom thickness facilitates low-noise operation.[57-61] Additionally, facile integration into large-scale circuit designs through existing

semiconductor device fabrication methods, ease of functionalization, and exceptional thermal and conductive properties[62,63] present an attractive biosensing platform.[59,64-66] Creating van der Waals heterostructures composed of various 2D material layers can enable structural and property engineering, while improving biosensor performance.

4.3. Functionalizing the Sensing Substrate

In designing interfaces between the operating environment and the sensing substrate, it is important to consider how molecules are presented on the surface in order to maximize intermolecular interactions. This includes considering the immobilization chemistry, biomolecule form and functionality, orientation geometry, and sensing strategy. Each aspect can therefore affect the strength of interaction between the probe and target, or the quality of signal transduction at the substrate-biorecognition interface. Thus, the method used for functionalizing the sensing surface can greatly affect the effectiveness of the biosensor.

Two-dimensional atomically thin materials can be functionalized two ways: covalent bonding and non-covalent bonding approaches. The former requires making chemical linkages between the probe and the substrate, whereas the latter relies on physisorption phenomena for probe immobilization. One consequence of covalent binding strategies on 2D materials are their disruption of the crystal lattice, which alter the physical and chemical properties and consequently its performance. For example, graphene when covalently linked with a molecule will cause sp^2 orbitals to become sp^3 bonds, as seen in its reduction to graphene oxide. Predicting and controlling the degree of sp^3 formation can present challenges in tuning graphene oxide performance.

Non-covalent functionalization has been performed using synthesized molecules. These types of immobilization capitalize on weak molecular forces such as van der Waals, hydrogen bonding, dipole-dipole interactions, and ionic bonds. Several classes of molecules have been used for non-covalent functionalization: polymers, aromatic molecules, and amphiphilic molecules.

Additionally, non-specific detection can misconstrue true sensing. Thus, it is important to prevent such incidences in order to maintain accurate readings. These occurrences can arise when off-target species, sample contaminants, or biological interferants interact directly with the sensing surface, typically when substrata are exposed directly to the environmental medium. One mitigation strategy is imparting anti-fouling properties to the sensing substrate thereby passivating it against non-specific interactions. Ideally, the sensor should display unresponsiveness when non-specific biological targets are introduced.

4.4. Solid-Binding Peptides for Sensor Functionalization

Solid-binding peptides (SBPs)[67-69] are short amino acid chains roughly 10-20 residues in length and have been used to interface organic and inorganic materials, functionalize various material surfaces, exhibit biocompatibility, and express inherent self-assembling properties. SBPs preferentially adsorb to specific substrates based on their amino acid sequence and their resulting secondary structures and peptide conformations, which can confer discrete functional domains that allow for strong surface binding, self-assembly, and displaying of moieties. The structural and chemical diversity of amino acids impart SBPs with multiple avenues for non-covalent interactions with the solid surface: electrostatic, polar, hydrophobic, and hydrogen bonding. These properties can be capitalized upon by functionalizing these SBPs with a variety of molecules, such as biosensing probes or enzymatic domains, to create novel bio-enabled devices **(Fig. 3)**.

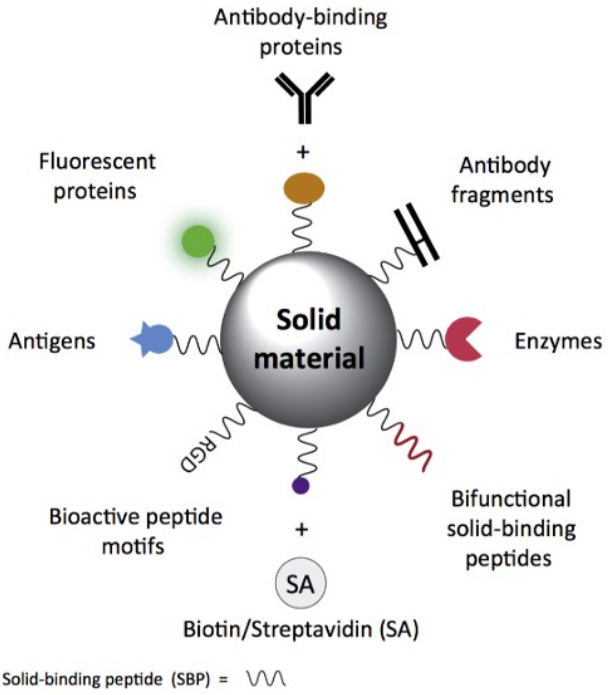

Figure 3. Multiple applications of solid-binding peptides. From Care et al. (2015).[68]

The use of SBPs opens up many options for using 2D materials as the sensing substrate—potentially delivering exotic device architectures that incorporate single-atomic layer conductors (e.g.,

graphene), semi-conductors (e.g., molybdenum disulfide), and insulators (e.g., boron nitride) to fully capitalize on their power and potential in biosensing applications. SBPs have shown selective adhesion to specific materials including graphene,[70] silica,[71,72] gold,[73,74] platinum,[75] titanium,[75] MoS_2, etc. This versatility grants flexibility to employ a variety of biosensing strategies, whether through field-effect transistors (FETs) that make use of 3D bulk or 2D layer substrates, or surface plasmon resonance (SPR) spectroscopy that require probe immobilization onto gold surfaces.

Taking advantage of graphene-binding peptides (GrBPs) developed in the lab to immobilize antibody probes, the research team has demonstrated a graphite-based sensor for detecting biotin-streptavidin interactions.[76] Additionally, non-specific adsorption of interferant proteins, metabolites, and off-target nucleic acid species are of major concern when testing clinically-relevant samples. Solid-binding peptides provide effective and inert, anti-fouling surface modification (i.e., passivation)—for example, preventing non-specific protein adsorption while still allowing specific detection of streptavidin against a background of bovine serum albumin.[76]

Moreover, doping single layer materials to control and enhance functionality is an extant challenge. Not only are dopant species distributed randomly on the surface, they also bind to single-layer substrates via covalent bonding—resulting in significant and unpredictable alteration of physical properties by disrupting the crystal lattice, thereby limiting its implementation in device applications. Previous research from this group has shown that challenges surrounding conventional doping can be circumvented by using SBPs as molecular dopants, which bind to 2D solids and predictively self-assemble on the surface. For example, GrBP can hole-dope graphene[70] through molecular recognition (i.e., assembly oriented along the crystal lattice) and affect charge transfer characteristics without compromising structural integrity of the 2D material. SBPs can therefore tune the conductance of single layer materials—allowing sensitive modulation of current-voltage behavior in FET-based biosensors.

Since miRNA biomarkers are the intended target, nucleic acid probes will be immobilized onto the sensing substrate. Peptide nucleic acids (PNAs)[77-79] are synthetic analogues of DNA, and were chosen

because they lack the negatively-charged phosphate group and instead possess an amine-carboxyl backbone—the same structure as peptide chains—that enables facile synthesis of peptide-PNA conjugates **(Fig. 4)**. Due to their synthetic backbone, PNAs possess 1) greater stability conferred by their resistance to nuclease and protease degradation; and 2) greater specificity towards RNA and DNA versus other types of nucleic acid interactions (c.f., DNA:DNA, DNA:RNA)[80] by averting backbone electrostatic repulsion upon hybridization. PNAs exhibit stronger duplex stability at higher temperatures,[81] sizeable thermodynamic instability under base-pair mismatching,[82,83] and can withstand low salt conditions[80,84] (unlike DNA-DNA and RNA duplexes)—contributing to superior specificity under high stringency conditions.[85]

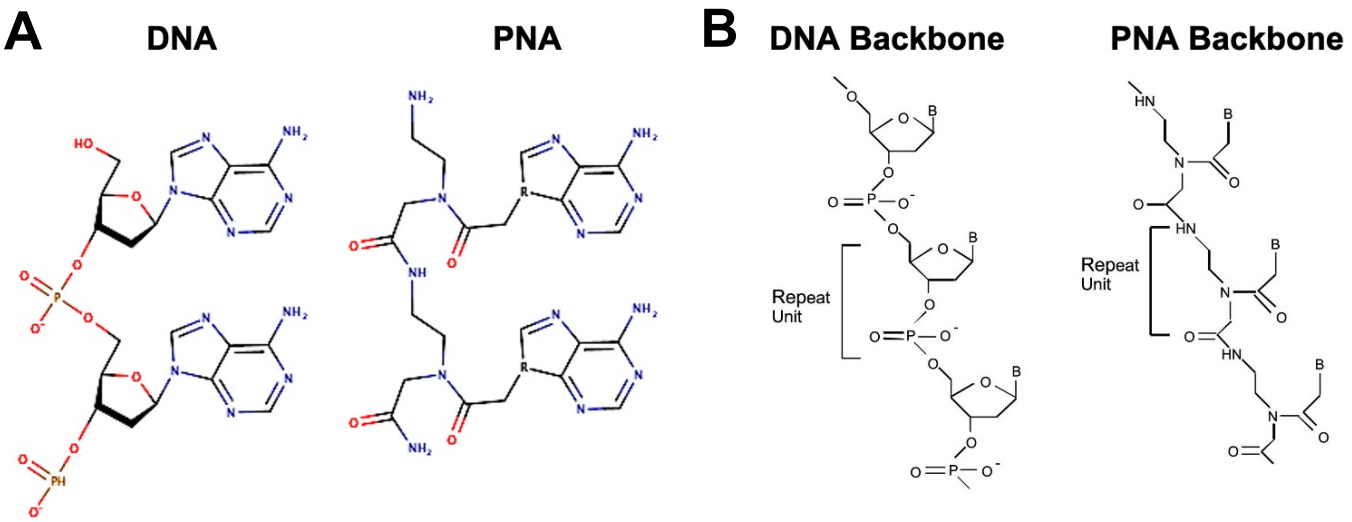

Figure 4. Comparison between DNA and peptide nucleic acid (PNA). (A) Nucleobases (e.g., adenine, cytosine, guanine, thymine) remains consistent between DNA and PNA molecules. **(B)** DNA is composed of a ribose-phosphate backbone, whereas PNA is entire made up of peptide linkages. Modified from Wang et al. (2004).[86]

To date there is no known instance of using solid-binding peptides to non-covalently immobilize PNA probes onto 2D single-atomic layer substrates. Although the aromatic molecule PBASE has been used to non-covalently secure probes onto sensing surfaces,[87] PBASE lacks the self-assembling properties inherent in SBPs that give rise to simple-to-complex nanoarchitectures[88] and allow spatial control of probe placement to optimize packing density—thereby enabling maximal target capture.

5. Motivation

5.1. Factors Limiting Early Detection of Pancreatic Cancer

Current detection methods[89] for pancreatic cancer include contrast-enhanced computed tomography (CT)[90] informed by endoscopic ultrasonography[91] with fine-needle aspiration (FNA) for observed lesions, as well as magnetic resonance imaging (MRI) and cholangiopancreatography.[92-94] Main drawbacks are their expensive and invasive nature. CA19-9[95-97] has long been used to confirm pancreatic cancer[98] and is the only FDA-approved biomarker recommended for monitoring disease progression.[99] However, by itself CA19-9 is insufficient for early diagnosis.[8,100,101] Key shortcomings are its lack of specificity and sensitivity—confounded by the presence of other diseases (e.g., non-malignant obstructive jaundice[102] and cholestasis[103]), as well as its absence in patients lacking Lewis antigens A and B.[104] Because of limitations on the predictive value of serum CA19-9 tests on asymptomatic patients, it is consequently impractical and economically prohibitive to routinely screen the general population.[105,106] Thus, screening has traditionally focused on those deemed at high risk. In light of these disadvantages, other kinds of biomarkers have been proposed for identifying and monitoring pancreatic cancer: metabolites,[107] glycoproteins,[108,109] and miRNAs.[40] Still, aside from CA19-9 assays, there are no established, standardized, clinically- or commercially-available methods that employ the use of biomarkers for early detection of pancreatic cancer.[110]

5.2. miRNA Biosensing for Early Detection, Diagnosis, and Prognosis

miRNA-based diagnostics do not yet exist. Conventional methods for detecting and quantifying miRNAs[111,112] are limited to qPCR,[113] microarray hybridization,[114-117] and NextGen sequencing.[118,119] These approaches involve lengthy extraction procedures, enzymatic amplification, subsequent fluorescent detection, and specialized personnel to operate expensive and sophisticated instruments, which do not readily lend themselves to convenient point-of-care analysis. Although microarrays provide high-throughput, comprehensive screening for a few thousand individual miRNAs to reveal global changes in

miRNA expression, limitations in sensitivity often necessitate pre-amplification procedures that can introduce non-linear inflation of miRNA or create biased amplification of certain species at the expense of others, requiring additional corrective analysis.[120,121] Furthermore, the reproducibility of microarray profiling is outmatched by low-throughput qPCR methods.[122] Thus, a strategic need exists for a robust biosensor platform to quantitatively detect miRNAs for diagnostic and prognostic purposes in pancreatic cancer aside from traditional oligonucleotide detection methods.

6. Approach & Methodology

In pursuing the development of a biosensor array against cancer miRNA biomarkers, several steps will be implemented. These include verifying the biomolecular sensing strategy, creation and characterization of the biosensor device, and expanding its capabilities to perform multiplexed detection of targets from biological samples **(Fig.5)**. Herein, research tasks are outlined which specify details, objectives, and considerations in meeting project goals.

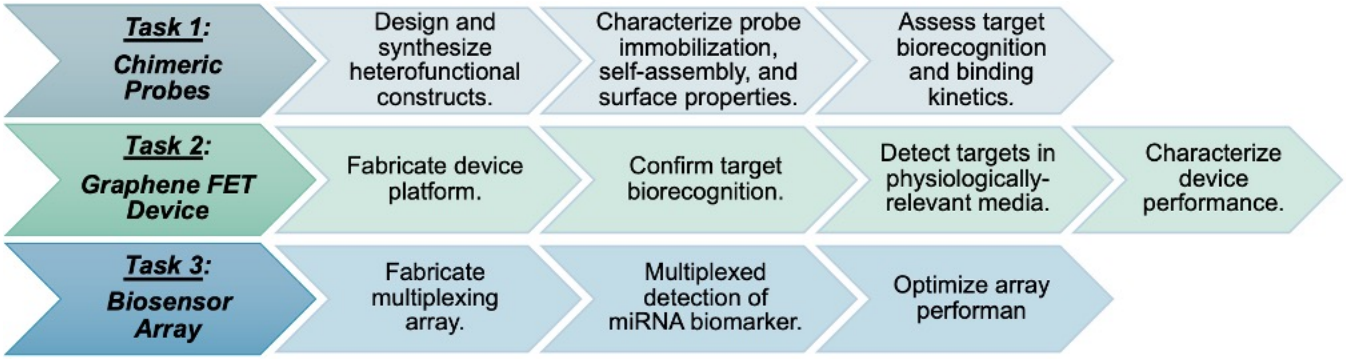

Figure 5. Research Strategy. Flow chart summarizing task areas towards development of cancer biosensor array against miRNA biomarkers.

6.1. Task 1: Design, Synthesis, & Characterization of the Chimeric Probe System

This aim seeks to establish and validate the heterofunctional modular sensing approach for nucleic acids using solid-binding peptides (SBP) and peptide nucleic acids (PNA)—focusing on probe immobilization, surface passivation, and hybridization. Anti-fouling (i.e., passivating) peptides will be used to protect exposed sensing surfaces from non-specific interaction with biological interferants.

Designed chimeric probes were assessed for target capture using SPR spectroscopy and quartz crystal microbalance techniques. Atomic force microscopy (AFM) was used to characterize the sensing surface following functionalization, with additional plans to carry out UV photoelectron spectroscopy and Raman spectroscopy.

6.1.1. Design and synthesis of heterofunctional SBP-PNA chimeric constructs.

Graphene-binding peptide and Chimeric GrBP-PNA. Graphene-binding peptide (N-terminus-IMVTESSDYSSY-C-terminus)[88] was prepared via standard FMOC solid-phase peptide synthesis and purified by high-performance liquid chromatography (HPLC). MALDI-TOF was done to confirm >95% purity. Chimeric GrBP-PNA construct (5'-aatgcgt-3'-SSIMVTESSDYSSY) was purchased commercially (PNA Bio, Newbury Park, CA, USA).

Gold-binding peptide and Chimeric AuBP-PNA. For validation studies requiring gold substrates, chimeras based on gold-binding peptides were used. Gold-binding peptide (AuBP) [123] bearing the amino acid sequence N-terminus-WAGAKRLVLRRE-C-terminus was synthesized using standard FMOC solid-phase peptide synthesis and purified via high-performance liquid chromatography followed by MALDI-TOF to confirm >95% purity. The chimeric AuBP-PNA construct (5'-tgaggct-3'-GGGWAGAKRLVLRRE) was purchased commercially (PNA Bio, Newbury Park, CA, USA) as well as the truncated probe (5'-agcctcaacccctatcac-3') and target (5'-ttaatgctaatcgtgataggggt-3') oligos (Integrated DNA Technologies, Coralville, IA, USA).

6.1.2. Probe immobilization, self-assembly, and surface characterization.

Peptide self-assembly. Synthesized heterofunctional chimeric constructs (e.g., GrBP-PNA) were incubated onto freshly-cleaved bulk highly-oriented pyrolytic graphite (HOPG), which consists of extended atomically-flat carbonaceous terraces and serves as a useful proxy for single-layer graphene. GrBP-PNA chimeras bind to HOPG and graphene surfaces through π-π stacking of the tyrosine-containing moiety with sp^2 hybrid orbitals of the substrate crystal lattice. Assembly characteristics were

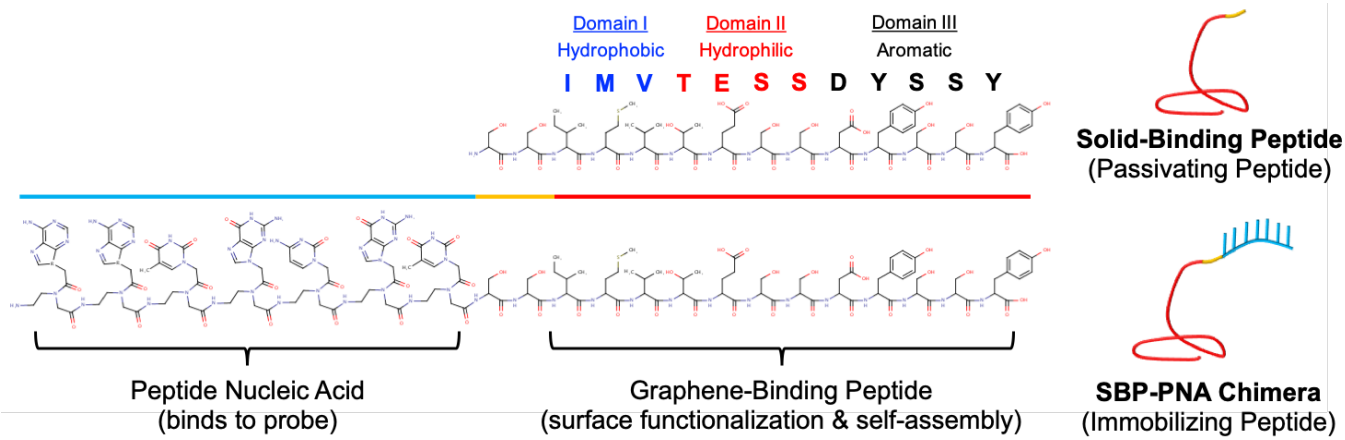

Figure 6. SBP and SBP-PNA chimeric constructs. Schematic showing molecular differences between the passivating solid-binding peptide that exhibits anti-fouling properties on graphene substrate, and chimeric SBP-PNA able to immobilize nucleic acid probes in order functionalize the graphene surface.

analyzed by atomic force microscopy (AFM) and assessed according to nanostructure morphology (height, surface coverage, etc.) and fold symmetry denoting molecular recognition of the substrate. Chimeric constructs (GrBP-PNA) were also co-assembled with anti-fouling passivating peptides (GrBP) to protect the sensing surface against non-specific adsorption at different percent ratios.

6.1.3. Functional studies for assessing target biorecognition and binding kinetics.

SPR analysis. Surface plasmon resonance (SPR) analysis was carried out on a Biacore T200 instrument (GE Healthcare, Pittsburg, PA, USA) on gold substrate (GE cat. BR100405). Chimeric AuBP-PNA, AuBP, DNA probe and DNA target samples were diluted in potassium phosphate buffer and passed at a flow rate of 50 µL/min. SPR studies will reveal surface densities of the adsorbed probe.[124,125] Binding kinetics will be determined for: 1) Adsorption of SBP-PNA chimeras to substrate; and 2) Biorecognition of nucleic acid targets to PNA probes. Assessing binding kinetics as a function of probe density[126,127] will reveal optimal incubation conditions for achieving high capture efficiency and maximal sensitivity.

QCM experiments. Functional tests with the chimeric and control constructs were carried out via quartz crystal microbalance (QSense, Biolin Scientific, Gothenberg, Sweden) on gold-coated quartz crystal electrode sensors (Biolin cat. QSX 301). Sensors were cleaned with Piranha solution (1:3 30% hydrogen peroxide:sulfuric acid) for <5 minutes, then rinsed with Milli-Q water and blow dried with N_2

gas. Flow-through concentrations of 10 μg/mL were used for AuBP-PNA chimeric peptide, AuBP peptide, truncated DNA probe, and DNA target. Peptide and DNA reagents were diluted in potassium phosphate buffer which also served as wash buffer for intervening steps. A flow rate of 100 μL/min was applied while temperature was set at 22.0 °C. The Sauerbrey relation ($\Delta m = -C \cdot \Delta f/n$) was used to calculate the total mass adsorbed where C=17.7 ng·Hz^{-1}·cm^{-2} for the 5 MHz quartz crystal and n=5 for the f5 harmonic overtone. Average dissipation was calculated from obtained D3, D5, D7, D9, D11, and D13 values corresponding to the respective harmonic overtones.

6.1.4. Alternative approaches to establish proof-of-concept detection.

Fluorescent and FRET microscopy on fluorophore-conjugated probes and targets can provide further qualitative and quantitative confirmation. Although quenching occurs when fluorescent molecules contact graphene, the presence of the peptide anti-fouling layer may prevent this while providing another metric for assessing graphene surface passivation. Additional validation techniques (e.g., electrochemical impedance spectroscopy on HOPG substrate, bio-layer interferometry on silica substrate using chimeras based on quartz-binding peptides) provide further proof of principle and evidence to the versatility of the SBP-PNA chimera approach for target capture and probe immobilization on a variety of sensing platforms.

6.2. Task 2: Detection of Nucleic Acid Targets by Graphene FET Devices

This aim seeks to assess nucleic acid detection against a background of physiological interferants (e.g., non-specific biomolecules found in biological fluids) using graphene FET testbeds functionalized with SBP-PNA chimeras. Doing so will inform the development of an array format to be used for multiplexed detection of multiple biomarker targets. The measurable output will be a change in the source-drain current resulting from hybridization of nucleic acid targets with immobilized anti-sense probes. This effect is commensurate with target concentration. Benchmarks for success include demonstrating sensitive and specific detection of a range of nucleic acid targets (e.g., DNA, miRNA) in simulated biological media (urine, blood, saliva, etc.) at physiologically relevant concentrations.

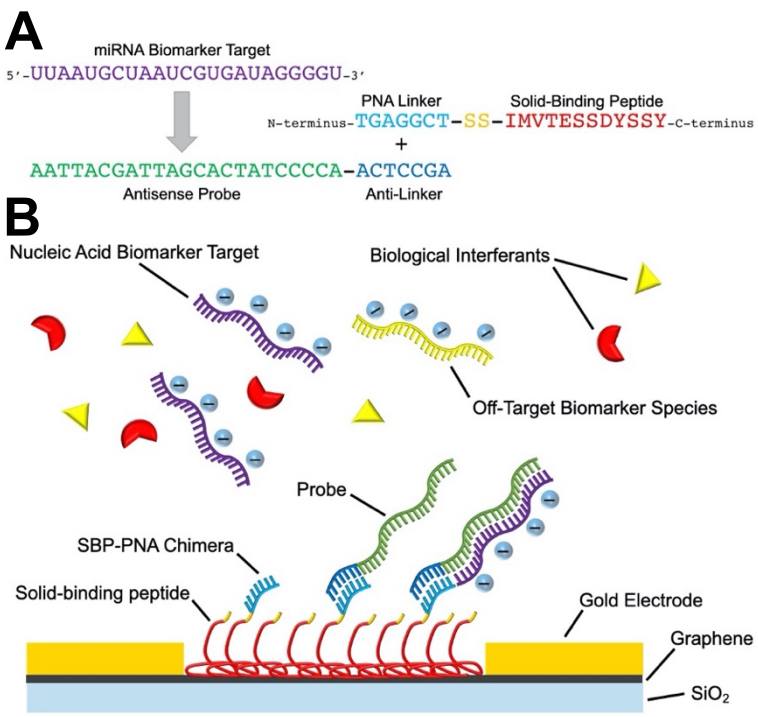

Figure 7. Biosensing Strategy. (A) Chimeric SBP-PNA constructs are specified to intended targets through hybridization of the PNA linker moeity with its complimentary anti-linker sequence of the antisense probe. The probe then binds to its biomarker compliment. **(B)** The graphene sensing surface is functionalized with a passivating SBP and a chimeric SBP-PNA that will immobilize a nucleic acid probe, which also hole-dopes the graphene material. The functionalized surface will then exhibit anti-fouling properties while maintaining binding capacity against specific miRNA targets. The target bears a highly negative charge due to its ribose-phosphate backbone, which perturbs the graphene sensing surface between the source-drain gold electrodes thereby eliciting a measurable change in electric current indicative of target capture.

6.2.1. Fabrication of the nanobiosensor platform.

GFET microfabrication. CVD-grown graphene transferred onto SiO_2 was purchased commercially (Graphenea) and underwent microfabrication processes in order to construct the sensor. Graphene patterning was accomplished via photolithography. AZ1520 positive photoresist was spin coated onto graphene at 3000 RPM then baked and exposed to UV (3.8 sec), followed by development in 4:1 AZ340:ddH_2O solution (60 sec) and washed in ddH_2O (60 sec). Reactive Ion Etching (RIE) was then performed followed by washing in acetone (65 sec) and isopronaol (80-90 sec). Gold electrode contacts were then added via metallization of a Cr bonding layer then Au. A final annealing step was carried out in 40%:60% hydrogen:argon gas mixture at 450 °C (1hr) to remove any residual surface contaminants. A short sonication process (5-10 minutes) was done to further remove any metallization. AFM and Raman spectroscopy was used to characterize the graphene surface.

6.2.2. Confirmation of target biorecognition.

Biosensing verification. Since RNA is highly prone to nuclease degradation, oligo DNA analogues of miRNA targets will be used in these initial studies. We will then probe for synthetic mature

miRNA oligonucleotides in an RNAse-free environment using RNAse-free reagents. Using the fabricated device, efficacy of nucleic acid detection by the chimeric SBP-PNA probes will be determined. Changes in graphene resistance are to be measured upon: 1) Formation of the modular probe (i.e., graphene functionalization); and 2) Hybridization of oligo targets (i.e., biorecognition). It is anticipated that both will result in decreased in GFET resistance since the target nucleic acids possess a negatively-charged backbone which may enhance hole-doping of the graphene substrate. Based on previous work, [76] the resistance drop is expected to be >50%.

6.2.3. Detection in physiological buffer.

Synthetic media. All experiments are to be carried out using oligonucleotide targets in DI water. In order to test detection at physiological osmotic and pH conditions, saline and buffered solutions are to be used. The urine, plasma, serum and saliva milieu will then be replicated by adding appropriate electrolytes, proteins, off-target biomarker species, and other potential interferants into the fluid environment. These experiments will assess how well the mixed SBP constructs and SBP-PNA chimeras can passivate and functionalize, respectively, the GFET sensing surface under physiological buffer conditions. Hybridization conditions such as ionic strength, temperature, and incubation time will also be altered to assess hybridization efficiency in both the presence and absence of physiological interferants.

6.2.4. Characterization of biosensor device performance.

Typical biosensor performance parameters[46] will be measured in order to assess device reliability and reproducibility. Device metrics will be characterized, such as dynamic range, signal-to-noise ratios, threshold voltage, current on/off ratio, charge carrier mobility, stability, and durability. Quantitative milestones include achieving:

Lower limit of detection (LLD) of <5 fM for target miRNA species along with single base-pair discrimination and p value <0.05 in biological buffers (plasma, serum, saliva, urine). This value aligns with physiological concentrations found in disease and healthy states. This will be accomplished by optimizing probe surface coverage, controlling hybridization temperature, and optimizing appropriate buffer solutions.

Linearity of response between 5 fM to 500 pM (i.e., linear range across six decades). This encompasses a broad range of physiological concentrations associated in healthy and disease states. The actual detection range will be between < 5 fM to 1 nM. We will perform nucleic acid dose response calibration curves (DNA, RNA, miRNA) to validate these ranges.

Sensitivity of >10 Siemens per fM across the linear range. This provides the current resolution needed to discriminate small absolute changes in miRNA expression (e.g., a 2-fold signal change over 5-20 fM change in target concentration) consistent with concentration differences of within 50-100 fM between normal and disease for circulating miRNA.

6.3. Task 3: Multiplexed Detection of miRNA Biomarker Targets by GFET Array

The goal is to create a sophisticated and sensitive nanobiosensor array to profile miRNA expression from healthy and disease-state samples of plasma, serum, saliva, and urine origin. Consequently, a nanobiosensor array with multiplexing capabilities would generate robust miRNA expression profiles that could readily distinguish disease conditions from healthy patients. A panel of selected miRNAs indicative of pancreatic cancer will be tested to determine the ability of the nanobiosensor array to successfully identify and distinguish early vs. late stages of disease.

6.3.1. Fabrication of the nanobiosensor array platform.

Individual GFET biosensors will be arranged into an array format with considerations into account for multiplexed electronic readouts and device packaging. A process flow yield >63% is sufficient—representing suitable scalability and reproducibility (e.g., 47 usable dies out of 75 produced per 4-inch silicon wafer) and corresponds to >92% yield for each fabrication step as defined by $(\text{Yield}_{\text{Cleaning}})\{(\text{Yield}_{\text{Photolithography}})(\text{Yield}_{\text{Etching}})\}^2(\text{Yield}_{\text{Deposition}})$ = Total Yield. Scanning electron microscopy will used to characterize device elements, while Raman spectroscopy will be used to determine the quality of the graphene sensing surface and its functionalization with peptide constructs.

6.3.2. Multiplexed detection of miRNA biomarker panels against pancreatic cancer.

Biological fluids supplemented with a panel of synthetic miRNA oligos will be used to test the biosensor array. Additionally, patient samples can be obtained from collaborators at the Fred Hutchinson Cancer Research Center in Seattle, WA, USA. Benchmarks for success include demonstrating measurement of a range of pancreatic cancer-associated miRNAs in various biological media at physiological concentrations relevant for early and late stages of disease, as well as at healthy conditions.

Several types of biological samples will be tested on the proposed nanobiosensor, but will start with urine because it contains less interferants than blood,[128] which could impact the sensitivity of the device. In addition, urine has already been used in the detection of bladder cancer miRNAs.[129] We will probe for early stage (miR-223, miR-204) and Stage I (miR- 143, miR-30e) pancreatic ductal adenocarcinoma (PDAC) miRNA biomarkers that are present in urine, which have been used in Affymetrix microarray analysis.[5] For detecting pancreatic cancer in early stages, we will also incorporate a plasma-derived miRNA panel[130] shown to have >95% sensitivity and specificity in diagnosing pancreatic ductal adenocarcinoma (PDAC): miR-10b, -30c, -106b, -132, -155, -181a, -181b, -196a, and -212. Early diagnosis will require taking into account risk factors (i.e., precursor legions[131,132]) that can precede PDAC, such as pancreatic intraepithelial neoplasia,[133] mucinous cystadenomas,[134] and intraductal papillary mucinous neoplasm (IPMN),[135] which themselves exhibit characteristic miRNA expression signatures.[136] For example, miR-1290 is associated with both IPMN and early stage PaC, while correlating higher expression with poorer outcome.[4] Both miR-155 and miR-21 are shown to be highly expressed in IPMN,[137] while the latter can predict patient survivability.[3,138] miR-196a is shown to parallel disease progression.[11]

6.3.3. Characterization of biosensor array performance.

The diagnostic efficacy of the array device will be determined, in addition to measuring typical performance parameters such as LLD, linearity of response, and analytic sensitivity. Quantitative milestones include achieving **clinical sensitivity** (true positive rate) and **clinical specificity** (true negative

rate) of >95% for Stage I and pre-Stage I samples, with a 95% confidence interval. This will be assessed by performing receiver operating characteristic (ROC) curves on the following sample sets in order to validate the diagnostic potential of the device: 1) Simulated biological media (e.g., urine, plasma, saliva, etc.) containing nucleic acid targets representative of healthy and disease states; and 2) Biological samples taken from normal and cancer patient cohorts. False discovery rates (FDR) of < 0.15 will be considered statistically significant. Current PCR-based assays show clinical sensitivities and specificities of 65-95+% depending on whether single or panel of miRNA biomarkers are used.[139]

6.3.4. Circumventing miRNA stability.

A potential challenge to detecting miRNAs in their native biological medium (serum, plasma, urine, saliva) is the presence of RNA binding proteins,[140-142] microvesicles,[143] and exosomes[144-146] that confer stability to circulating miRNAs, which may hinder hybridization of target species to the probes. Still, whether exosomal miRNA contributes substantially to the overall circulating miRNA population has been called into question.[147] Samples may, therefore, require pre-treatment with appropriate buffers to release miRNAs from their respective biological binding partners, or need purification using commercially-available miRNA extraction kits. For example, RNA-binding protein immunoprecipitation (EMD Millipore, Billerica, MA, USA) may need to be performed to rule out target species shown to be bound to binding proteins. The incorporation of lab-on-a-chip microfluidic designs can also be explored to allow for miRNA isolation prior to detection.[148]

7. Results & Analysis

7.1. Results for Task 1: The Chimeric Probe System

Heterofunctional SBP-PNA constructs that act as probe immobilizers for functionalizing graphene surfaces for GFET biosensors, and gold substrates in SPR and QCM validation studies, were designed by imparting solid-binding peptides with a peptide nucleic acid moiety. In addition, regular SBP constructs (i.e., graphene-binding peptide, gold-binding peptide) were used to passivate exposed sensor surfaces for

protection against non-specific binding. In using both types of peptides, their miscibility and functionality were assessed prior to implementing the chimeric peptide approach onto the biosensor device.

7.1.1. Overcoming Phase Separation Between Chimeric and Passivating Peptides.

Since two types of peptides (i.e., SBP and SBP-PNA) were used each having differing molecular weights and molecular constitution, then it is important to consider their compatibility and miscibility to ensure that one does not interfere with the other regarding their functionality (anti-fouling vs. probe immobilization). For example, aggregation of a peptide species can cause diminished biorecognition efficacy due to steric hindrance effects that preclude access to molecular binding sites. Thus, the effects of peptide concentration and phase formation was investigated.

Incubation of 1 uM passivating graphene-binding peptide (GrBP5) onto HOPG substrate results in ordered structures displaying six-fold symmetry—indicating molecular recognition of tyrosine residues in the solid-binding peptide with the underlying graphite crystal lattice **(Fig. 8)**. Because this peptide does not bear the PNA moiety, it is used solely for anti-fouling purposes to protect the sensing surface from non-specific adsorption. In contrast, the chimeric graphene binding peptide-PNA (GrBP-PNA) construct results in amorphous assembly on HOPG. The lack of long-range ordering may be caused by the high aromaticity content of nucleobases present in PNA, which may form π-π stacking with delocalized sp^2 electrons of the carbon substrate. Thus, it is likely that at low surface densities, the chimeric construct does not display the PNA moiety in an upright fashion, but rather in a longitudinal orientation parallel to the substrate surface. That is, PNA probes may bind directly to graphene and prevent proper probe display. This is evidenced when comparing height profiles of passivating and chimeric peptides whereby both exhibit similar heights (approximately 1.3 nm) when assembled at low concentrations. However, data reveal that such undesired immobilization can be prevented by mixing SBP-PNA chimeric constructs with increasing amounts of passivating SBPs.

When combining chimeric GrBP-PNA with passivating GrBP, discrete domains of ordered and

amorphous regions are observed. However, at higher concentrations (2 uM) of mixed peptides reduces this phase separation whereby GrBP-PNA chimeras seem to become miscible with regular SBPs. Thus, self-assembly may be tuned by altering percent composition of mixtures to allow for controlled functionalization of the sensing surface. Optimizing the percent composition ratio of SBP:SBP-PNA mixtures may have promoted proper probe display through co-assembly since doing so probably constrains the chimeric construct (SBP-PNA) to adopt self- assembly characteristics of the passivating peptide (SBP). These approaches are analogous to using 11-mercapto-1-undecanol (short alkylthiol surface diluent) or 6-mercapto-1-hexanol (spacer thiol) to backfill thiol-derivatized DNA monolayers on gold.[149] These alkylthiols displace weak nucleobase nitrogen-gold interactions (i.e., non-specifically-adsorbed DNA) from the gold surface and reorients the probe to a more upright position due to electrostatic and steric hindrance effects.[149,150]

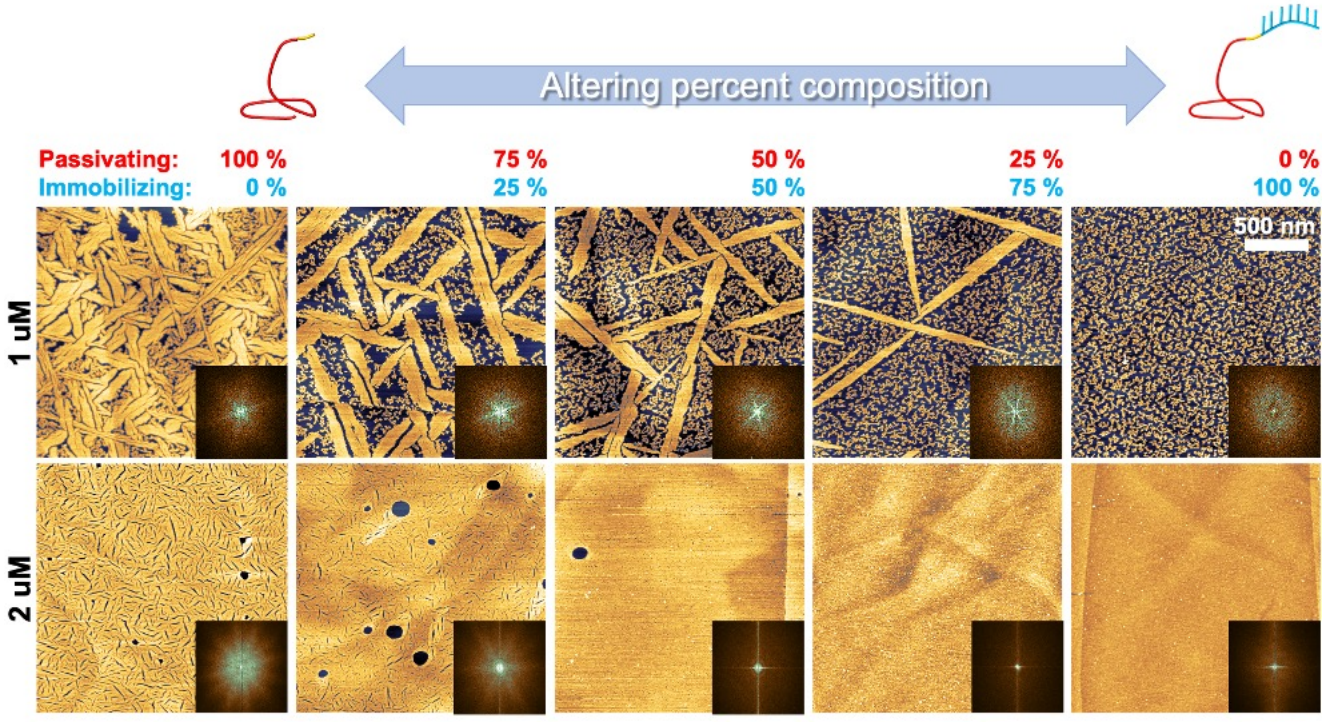

Figure 8. Tuning miscibility of anti-fouling and chimeric peptides. AFM images of peptide assembly on HOPG substrate show that at lower 1 uM concentrations, long range ordering by the passivating Graphene-binding peptide is reduced as increasing percent concentration of GrBP-PNA is added. However, at higher 2 uM concentrations, both peptides show loss of domains and phase separation, indicating complete mixing to form monolayer with few exposed substrate surfaces.

Tuning the surface distribution of chimeric SBP-PNA constructs alongside passivating solid-binding peptides would help implement a more reliable biosensing interface. Uncontrolled surface coverage of concentrated chimeric regions (i.e. domains) can lead to inconsistent surface functionalization and result in variable sensor responses. Likewise, if the chimeric construct exhibits suboptimal packing density (i.e. overcrowding), then steric hindrance and electrostatic repulsion—caused by the negatively-charged ribose-phosphate backbone of nucleic acids—may diminish hybridization efficacy between the immobilized probe and biomarker target. Thus, it is important that miscibility is properly achieved between the passivating and chimeric peptides in order to yield both a robust biorecognition event and consistent surface functionalization between devices.

7.1.2. Nucleic Acid Detection by Chimeric SBP-PNA Constructs

The versatility of the chimeric probe system is its modularity, in that the solid-binding peptide component can be replaced by a different peptide while still maintaining the facile ability to immobilize the same probe—but on a different surface. In validating the probe immobilization process and subsequent target capture, two methods were used to assess biomolecular interactions: Surface plasmon resonance (SPR) and quartz crystal microbalance (QCM) analysis. However, these approaches require using a gold substrate for adsorption of the solid-binding peptide. Thus, a second SBP-PNA chimeric construct was used—one based on gold-binding peptide.

The steps involved include 1) surface adsorption of the chimeric and anti-fouling constructs, 2) immobilization of the nucleic acid probe onto the surface, and 3) capture of the target **(Fig. 9A)**. The first two steps are essentially surface functionalization of the gold substrate, which was accomplished by flowing through peptide solution. Following probe immobilization, a buffered solution containing the target was flowed and the biorecognition event quantified.

In a typical SPR setup, light shining on a gold surface at a critical angle with a certain wavelength can be absorbed by the gold conduction electrons (rather than being reflected off the surface) whereby the absorbed energy induces their oscillation **(Fig. 9B)**. This surface plasmon resonance effect is sensitive in

which accumulating adsorbates on the gold surface causes a measurable shift in the SPR wavelength (i.e., the absorbed wavelength red shifts). This phenomenon was used to validate the chimeric probe approach.

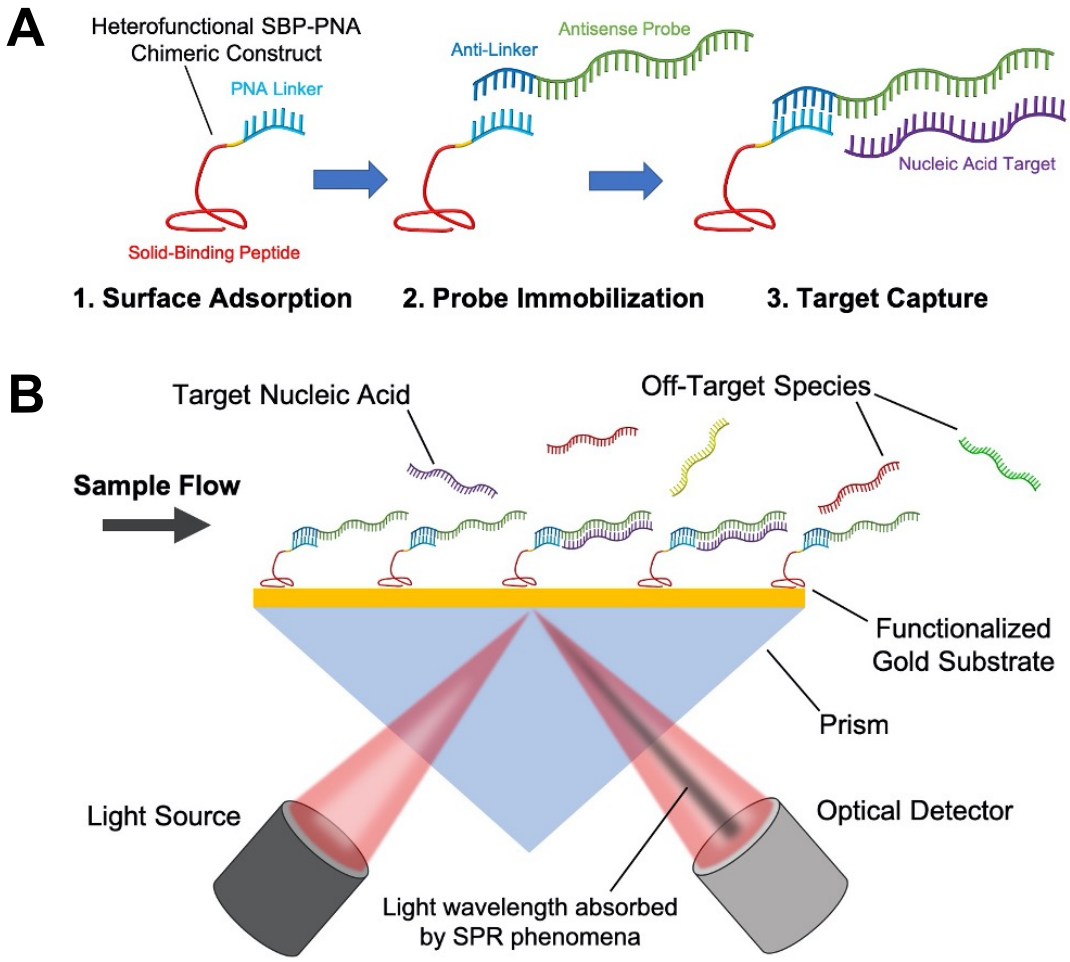

Figure 9. SPR experimental paradigm. (A) Schematic depicting stages of surface functionalization and detection. First chimeric SBP-PNA is adsorbed onto material surface, then nucleic acid probes are immobilized onto the surface, followed by detection of target. **(B)** Diagram illustrating specific capture of nucleic acid targets on functionalized SPR gold surface and resulting shift in absorbed SPR wavelength.

SPR spectroscopy reveals that the AuBP-PNA construct adsorbed onto the gold substrate as evidenced by the increasing SPR shift upon repeated flow through of the peptide **(Fig. 10A, green)**. Loosely bound chimeric peptides were removed using intermittent buffer wash steps showing a concomitant decrease in the SPR shift response. Afterwards, the DNA probe was introduced by flow through which also resulted in increasing SPR shifts, but with minimal changes during washing steps **(Fig. 10A, pink)**. This suggests that the probe is tightly bound through the PNA linker—anti-linker interaction.

After demonstrating surface functionalization on gold by immobilizing chimeric AuBP-PNA constructs, SPR was used to show capture of a nucleic acid target **(Fig. 10B, green arrows)**. These studies also reveal that a 1:9 percent mixture of chimeric peptdie to passivating peptide is optimal for effective capture of DNA target at 750 nM since SPR response amplitude is greater at reduced probe packing densities. This is likely due to reduced steric hindrance creating more accessible space between the immobilized probes, along with minimizing electrostatic repulsion between neighboring bound targets and their negatively charged backbones. The effect of probe packing density has been investigated and it is predicted that of ~2 x 10^{12} molecules/cm^2 would yield >90% hybridization efficiency.[126]

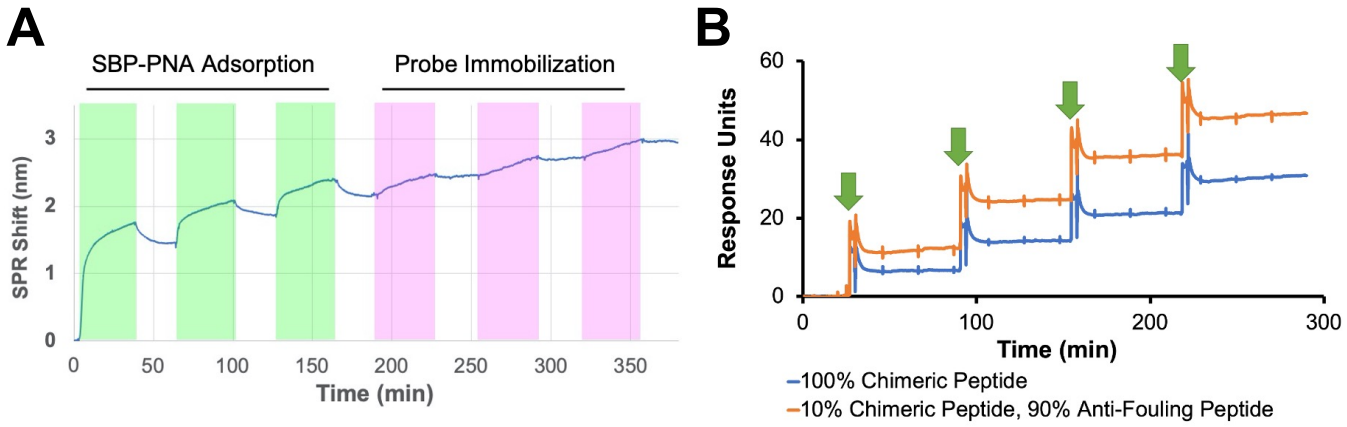

Figure 10. Surface functionalization and target capture by chimeric gold-binding peptide-PNA construct. (A) SPR analysis shows AuBP-PNA adsorption (green) onto gold surface followed by hybridization with DNA probe (pink). **(B)** SPR profile confirming detection of target after surface functionalization. Repeating flow through of target results in increasing SPR response (green arrows). Data also reveal that mixing immobilizing (chimeric) and passivating (anti-fouling) peptide shows greater biorecognition efficacy versus chimeric peptide alone.

Quartz crystal microbalance (QCM) experiments were also carried out to monitor the sequential formation of the sensing chimeric assembly—adsorption of the peptide followed by immobilization of the probe. The working principle behind QCM is that a piezoelectric quartz crystal oscillates at a steady resonant frequency. However, upon accumulation of adsorbates onto its gold-coated surface, its oscillation frequency will dampen in response to the added mass. This physical characteristic allows for accurate measurement of mass buildup in response to peptide surface adsorption, probe immobilization, and target capture. Three solutions were tested: 1) Anti-fouling AuBP (passivatng peptide), which served as a control

since it lacks the PNA moiety and therefore cannot immobilize the probe; 2) Chimeric AuBP-PNA (immobilizing peptide); and 3) a mixture of both peptides at a 1:1 ratio. After adsorption, the probe was flowed through, and then the target—for all three conditions.

Flowing through the peptides over the gold-coated QCM sensor showed a decrease in resonant frequency for the chimeric AuBP1-PNA construct and AuBP1-only samples, demonstrating mass accumulation at the sensor surface as the peptide adsorbs onto the gold substrate and diminish the oscillation speed **(Fig. 11A, green, blue)**. From the Sauerbrey relation, it was determined that 43.4 ng PNA-AuBP1 and 21.2 ng AuBP1 adsorbed onto the surface. However, despite the more robust response for the chimeric peptide because of its larger molecular weight (3557.7 vs. 1454.7 g/mol), the number of adsorbed molecules were similar for both conditions (12.19 and 14.57 pmoles, respectively). This implies that both the immobilizing and passivating peptide occupy the same footprint space such that the PNA linker remains upright and displayed properly rather than lying flat on the surface.

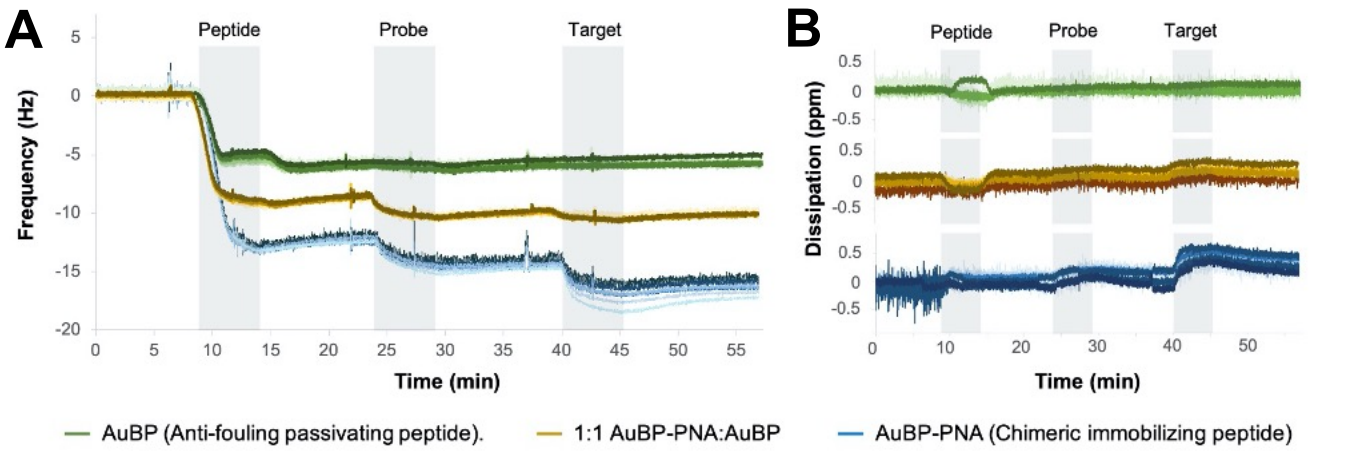

Figure 11. Sequential assembly of the chimeric probe system. (A) QCM spectra showing decrease in resonance frequency as mass is adsorbed to surface suggesting that surface is becoming functionalized and target is being captured. **(B)** QCM-Dissipation data reveals greater loss of dissipation energy for the chimeric immobilizing peptide upon probe immobilization and binding with target indicating that a flexible viscoelastic layer is formed, but absent in the anti-fouling-only layer.

Flowing through the nucleic acid probe onto the adsorbed chimeric construct resulted in a further decrease in frequency corresponding to 8.33 ng (1.56 pmole) probe being immobilized onto the gold surface. In contrast and as expected, this frequency shift was absent for the AuBP1-only condition since

it cannot hybridize the DNA probe owing to its lack of the PNA moiety. Under the chimeric peptide condition, presenting the target to the immobilized probe further decreased the QCM frequency. This indicates DNA was captured by the probe and corresponds to 6.48 ng (0.91 pmole) target bound to the chimeric complex. This effect was again absent for the AuBP1-only condition.

For the 1:1 ratio of mixed peptides, the sensor response was intermediate between the two previous conditions **(Fig. 11A, brown)**. It is interesting to note that the target response was not enhanced for this condition despite expectations that a lower probe packing density would foster greater target capture due to reduced steric hindrance and electrostatic repulsion. This may be explained by the fact that the chimeric peptide is more than twice the mass as the anti-fouling peptide. Thus, the expected larger reduction in resonant frequency resulting from more effective target capture may have been offset by the reduced mass incurred due fewer chimeric constructs on the surface.

QCM data accounting for kinetic dissipation of biomolecules (QCM-D) reveal a thin and rigid layer during chimeric peptide and probe steps as evidenced by, firstly, overlapping and coincident dissipation profiles for all overtones and, secondly, their values still being close to zero following adsorption and immobilization (average ΔD=0.06±0.011 and 0.09±0.027, respectively) **(Fig. 11B, blue)**. However, during the target capture step, the average change in dissipation increases much greater (ΔD=0.23±0.022) suggesting more viscoelasticity of the formed layer upon sequential DNA hybridization. That is, a once rigid layer has now become softer, which may be explained by the creation of a larger nanostructure composed of a flexible DNA probe anchored to the SBP base followed by the addition of a flexible nucleic acid target upon biorecognition to the probe. This effect is much reduced in the 1:1 mixed ratio, and is absent in the AuBP-only condition which does not bind the target.

7.2. Results for Task 2: Graphene FET Devices

7.2.1. Fabrication of GFET biosensor.

Graphene biosensor testbeds were fabricated according to the described process flow in which a

die was produced consisting of eight individual sensors **(Fig. 12A,B)**. Using this high throughput microfabrication strategy—in lieu of manual bulk graphite exfoliation in order to isolate single-layer graphene samples—illustrates a facile approach for creating the biosensor array for multiplexed detection. Still, the fabrication process must be further optimized to achieve higher die yields since some sensors displayed tearing of the graphene sheet, incomplete removal of discarded electrode components, and inadvertent surface abrasion **(Fig. 12C, black arrows)**.

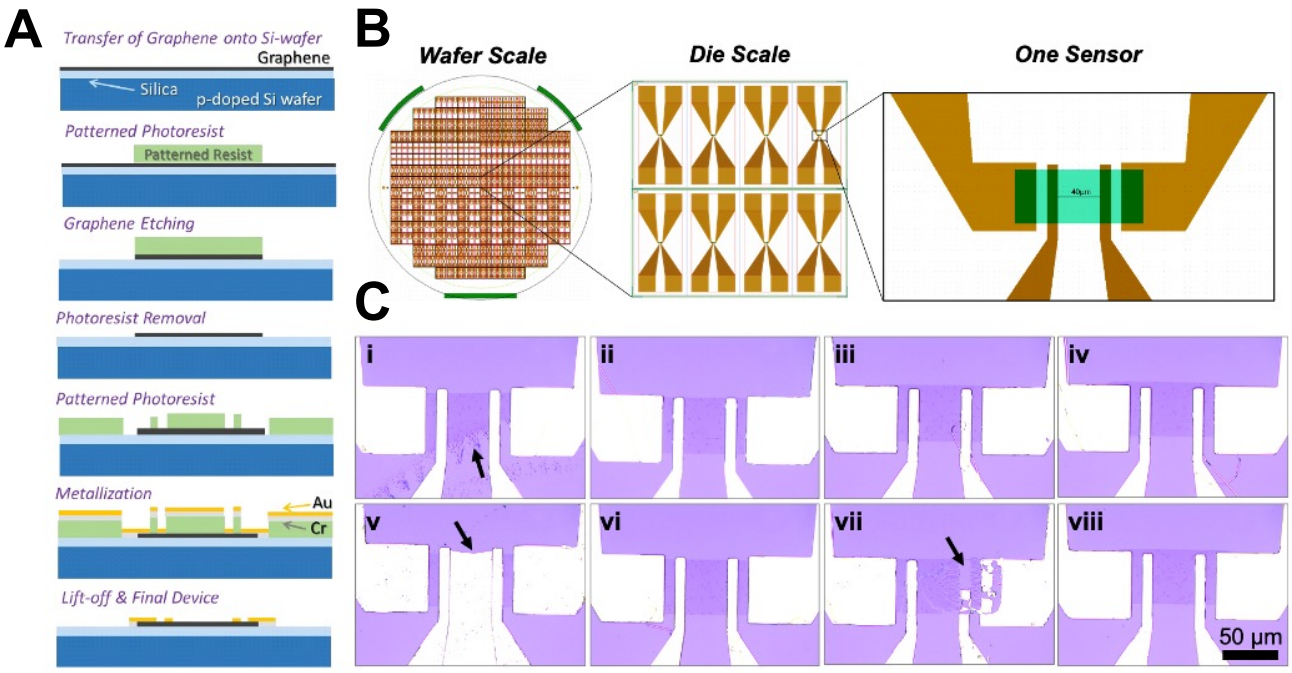

Figure 12. Fabrication of Graphene FET testbed. (A) Microfabrication process flow of GFET device. **(B)** Schematic illustrating high-throughput manufacture of graphene sensors arranged on 4-inch silicon wafer. Brown color represents gold contacts, mint green color represents patterned graphene. **(C)** Optical images of fabricated graphene biosensors at the die scale displaying pristine and faulty (black arrows) qualities.

Raman spectroscopy was performed[151] to confirm graphene integrity following microfabrication processes. As a point of reference, single-layer graphene was produced by mechanical exfoliation and confirmed by optical microscopy,[152,153] Expectedly, a short G-band at 1583 cm^{-1} and an intense sharp 2D band between 2500-2800 cm^{-1} was observed on single-layer exfoliated graphene. The amplitude of the 2D band diminishes with increasing graphene layers thereby altering the G:2D band ratio as follows: 1:1 relative height for double layer, 2:1 relative height for triple layer, and 3:1 relative height for bulk graphene

(Fig. 13A). In comparison, Raman spectroscopy on the CVD-grown graphene following photolithographic patterning showed similar G and 2D band amplitudes corresponding to predominantly single- layer graphene with no other significant peaks indicating a pristine graphene surface **(Fig. 13B).** Raman spectroscopy on microfabricated graphene biosensors having undergone photolithography, etching, metallization, and annealing also showed prominent G and 2D peaks **(Fig. 13C)**. While the two peaks are characteristic of graphene, the amplitude ratio of the two peaks seem now more consistent with double layer than single layer. This difference may have arisen during the annealing step. Optical microscopy and AFM reveal a pristine surface suitable for functionalization (data not shown).

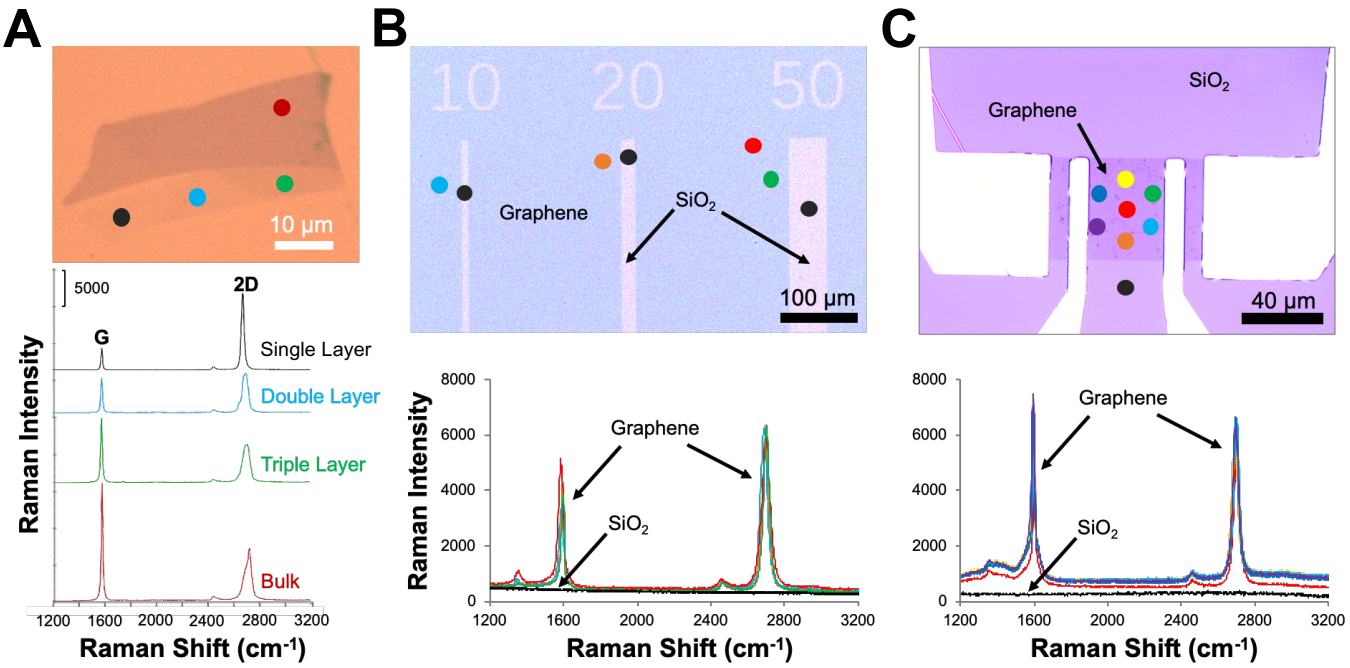

Figure 13. Comparison of graphene quality after processing. (A) Optical image of exfoliated graphene on SiO_2 with single and multilayers. Raman spectroscopy shows expected G and 2D bands for single, double, and triple layers versus bulk. **(B)** Optical image of transferred CVD-grown graphene on SiO_2 following photolithography process. Raman spectroscopy reveals mostly single-layer graphene. **(C)** Optical image of graphene sheet following complete microfabrication process of photolithography, metallization, and annealing.

7.1. Results for Task 3: Multiplexed Detection of miRNA Targets

7.1.1. miRNA biomarker panel candidates identified.

In selecting candidate targets, it was considered whether reported miRNA biomarkers were

detected from tissue,[135,154] serum,[1,3,4,155,156] plasma,[11,157-160] saliva,[2] or urine[5] since expression discrepancies exist between tissues and bodily fluids[154] **(Table 1)**. Accounted was whether studies had reported averaged data from a cohort of combined Stage I-IV patients,[156,157] or used pooled heterogeneous samples,[3,161] as this may compromise how well the biomarkers can distinguish early-stage from late-stage disease. Microarray expression data[162,163] submitted to the Gene Expression Omnibus[164-166] database can also be mined to seek out unique pancreatic cancer miRNA signatures (e.g., series accession numbers GSE2564,[167] GSE25820,[168] GSE59856,[1] GDS4329,[169] GDS4103,[170] GDS4102,[171] GDS4100,[172] etc.). This can provide an additional source of targets from disease-state miRNA expression profiles that can be further validated using receiver operating curves.

Table 1. Identified miRNA biomarkers against pancreatic cancer.[1-5,135,154-160]

Sample	miRNA	Sequence
Serum*	miR-20a	UAAAGUGCUUAUAGUGCAGGUAG
Serum*	miR-21	UAGCUUAUCAGACUGAUGUUGA
Serum*	miR-24	
Serum*	miR-25(-3p)	CAUUGCACUUGUCUCGGUCUGA
Serum	miR-34a	UGGCAGUGUCUUAGCUGGUUGU
Serum*	miR-99a	AACCCGUAGAUCCGAUCUUGUG
Serum	miR-125a-3p	ACAGGUGAGGUUCUUGGGAGCC
Serum	miR-134(-5p)	UGUGACUGGUUGACCAGAGGGG
Serum	miR-146a(-5p)	UGAGAACUGAAUUCCAUGGGUU
Serum*	miR-185(-5p)	UGGAGAGAAAGGCAGUUCCUGA
Serum*	miR-191(-5p)	CAACGGAAUCCCAAAAGCAGCUG
Serum	miR-200a(-3p)	UAACACUGUCUGGUAACGAUGU
Serum	miR-200b(-3p)	UAAUACUGCCUGGUAAUGAUGA
Serum	miR-378	
Serum	miR-484	UCAGGCUCAGUCCCCUCCCGAU
Serum	miR-628-3p	UCUAGUAAGAGUGGCAGUCGA
Serum	miR-770-5p	UCCAGUACCACGUGUCAGGGCCA
Serum	miR-1290	UGGAUUUUUGGAUCAGGGA
Serum	miR-1303	UUUAGAGACGGGGUCUUGCUCU
Serum	miR-1825	UCCAGUGCCCUCCUCUCC
Serum	miR-4294	GGGAGUCUACAGCAGGG
Serum	miR-4476	CAGGAAGGAUUUAGGGACAGGC
Serum	miR-4530	CCCAGCAGGACGGGAGCG
Serum	miR-6075	ACGGCCCAGGCGGCAUUGGUG
Serum	miR-6799-5p	GGGGAGGUGUGCAGGGCUGG
Serum	miR-6836-3p	AUGCCUCCCCCGGCCCCGCAG
Serum	miR-6880-5p	UGGUGGAGGAAGAGGGCAGCUC

Sample	miRNA	Sequence
Plasma	miR-16	
Plasma	miR-18a(-5p)	UAAGGUGCAUCUAGUGCAGAUAG
Plasma	miR-21(-5p)	UAGCUUAUCAGACUGAUGUUGA
Plasma	miR-155(-5p)	UUAAUGCUAAUCGUGAUAGGGGU
Plasma	miR-181a	
Plasma	miR-181b	
Plasma	miR-196a	
Plasma	miR-210(-5p)	AGCCCCUGCCCACCGCACACUG
Plasma	miR-221(-3p)	AGCUACAUUGUCUGCUGGGUUUC
Plasma	miR-375	UUUGUUCGUUCGGCUCGCGUGA
Plasma	miR-483-3p	UCACUCCUCUCCUCCCGUCUU

Sample	miRNA	Sequence
Urine	miR-30e(-5p)	UGUAAACAUCCUUGACUGGAAG
Urine	miR-143(-3p)	UGAGAUGAAGCACUGUAGCUC
Urine	miR-204	
Urine	miR-223(-3p)	UGUCAGUUUGUCAAAUACCCCA
Urine	miR-483-5p	AAGACGGGAGGAAAGAAGGGAG
Urine	miR-665	ACCAGGAGGCUGAGGCCCCU
Urine	miR-3663-3p	UGAGCACCACACAGGCCGGGCGC

Sample	miRNA	Sequence
Saliva	miR-1246	AAUGGAUUUUUGGAGCAGG
Saliva	miR-4644	UGGAGAGAGAAAAGAGACAGAAG

8. Discussion

Several key attributes must exist to detect ultra-low miRNA concentrations in biological fluid: 1) Probes immobilized onto 2D-layer substrates must not compromise structural integrity or electronic properties of the sensing material; 2) Optimal probe density must be achieved for efficient target capture in order to avoid steric hindrance of probes or electrostatic repulsion of charged targets; 3) Non-specific adsorption of biological and chemical interferants must be mitigated to prevent erroneous effects on the 2D sensing substrate, which can cause false positives readings; and 4) Non-covalent probe attachment is favored to minimize defects in the underlying crystal lattice of the sensing material which could alter sensing properties.

In the present study, chimeric PNA-SBPs were used to anchor nucleic acid probes onto either graphitic or gold substrates for characterizing self-assembly and validation of nucleic acid detection, respectively. Heterofunctional constructs composed of solid-binding peptide and peptide nucleic acid were used to facilitate detection of nucleic acid targets onto various sensor surfaces. For gold-binding peptide chimeras, quartz crystal microbalance (QCM) was used to demonstrate the sequential biomolecular assembly of the modular chimeric probe system, while surface plasmon resonance (SPR) spectroscopy revealed the effect of steric hindrance on target capture whereby a lesser probe packing density results in greater sensitivity. The results of using two different heterofunctional constructs—one based on graphene-binding peptides and the other based on gold-binding peptides—demonstrate the versatility of a modular approach to sensor surface functionalization by allowing probe immobilization onto various sensing materials, as well as the viability of using such SBP-PNA chimeric molecules for capturing nucleic acid targets (e.g., miRNAs, cell-free DNA) thereby creating a path towards defect-free functionalization of 2D materials by non-covalent means.

Key aspects of designing effective biosensors include tethering probes onto the sensing substrate while maintaining their proper orientation to appropriately bind target molecules, and efficient signal

transduction across soft bio/nano interfaces of the sensing surface. Solid-binding peptides present a suitable method for non-covalent immobilization of probes onto single-atomic layer substrates. This approach delivers functionalization while eschewing the challenges posed by covalent modification, such as the introduction of lattice defects that could adversely affect sensing properties, for example, by creating cause electron scattering points, and is therefore especially relevant to sensors based on two-dimensional materials like graphene and MoS_2.

However, in order for a biosensor to be truly effective, it must be able to detect targets from biological samples. Sensing biomolecules in their native environment can offset complications caused by loss of tertiary and secondary structures due to changes in the solution ionic strength (i.e., protein denaturation) when biological samples are diluted. For example, the presence of salt has also been shown to provide a stabilizing effect on protein conformations. [173] Other issues related to diluting biological samples is that decreased detection of the target species can occur due to a reduced target load in the media. In addition, operator error may also lead to inconsistent reproducibility because of additional manual handling of the sample. In addition, DNA hybridization does require the presence of ionic salts to dampen electrostatic repulsion between the negatively-charged ribose phosphate backbones of sense and antisense strands. [174] Conversely, PNAs can withstand high stringency conditions (i.e., low ionic strength) better than DNA or RNA, and because PNAs exhibit greater thermal stability, these characteristics allow for higher sensitivity and specificity for the target nucleic acids despite detecting in a low-salt environment.

However, the presence of ions can also interfere with the sensitivity of a biosensor by decreasing the Debye length of the sensing channel whereby charge screening effects from ions in solution affect the signal transduction of molecular interactions at the sensor surface. The greater the ionic strength of the solution environment, the lower the Debye length due to larger charge screening. Thus, ionic strength of solution can interfere with signal transduction at the FET interface. This becomes especially important in salt buffers such as PBS and physiological biological fluids since the media environment may affect

structural and functional properties of both the solid binding peptide as well as the probe, in addition to biomarker targets. Though this phenomenon presents an opportunity for using solid-binding peptides to fine tune local Debye lengths along the sensing channel to improve sensitivity and strength of signal transduction.

9. Future Plans

The proposed research project describes three aims towards developing a nanobiosensor array for miRNA profiling from biological samples: 1) Design, Synthesis, & Characterization of the Chimeric Probe System; 2) Detection of Nucleic Acid Targets by Graphene FET Devices; and 3) Multiplexed Detection of miRNA Biomarker Targets by GFET Array.

9.1. Addressing Task 1: The Chimeric Probe System

The subtasks associated with Task 1 are largely complete—culminating with a proof-of-principle detection of nucleic acid targets.

9.1.1. Probing the biomolecular interaction at the substrate-solution interface.

However, additional characterization of the physical phenomenon occurring at the substrate-biomolecular interface can reveal criteria and insight for adequate probe immobilization, optimal probe density, and surface passivation (e.g., surface diffusion, substrate doping, uniformity control). For example, electron transport properties can be measured using conductive AFM by comparing bare graphene surface, functionalized surface, and captured target conditions. This could provide insight into how the negatively-charged backbone of nucleic acid targets affect the source-drain current across the graphene sensing channel, especially since graphene becomes doped with positive hole charge carriers upon adsorption of solid-binding peptides.

Ultraviolet photoelectron spectroscopy (UPS) of graphene[151] before and after probe immobilization could further reveal the hole-doping effect via a change in the measured work function (approx. 0.3 eV increased shift). Raman spectroscopy would confirm[151] graphene passivation, probe

immobilization, and biorecognition of the nucleic acid target. It is expected that the Raman spectrum of bare graphene (1583 cm^{-1} G-band with an intense sharp 2500-2800 cm^{-1} 2D band) will change from two peaks to an increasing number of peaks as the SBP-PNA chimeric construct immobilizes the probe and nucleic acid targets are captured. These studies will yield a fundamental understanding of how peptide-substrate interactions influence nanomaterial properties to affect sensitivity and specificity of cancer biomarkers. The obtained results will also further inform the use of peptide-enabled single-atomic layer materials at bioelectronic interfaces.

9.1.2. Tackling peptide desorption.

Bovine serum albumin (BSA) is often used to passivate surfaces due to its high molecular weight rendering it unlikely to be displaced by other proteins. However, its large size also poses challenges for surface functionalization since the resulting steric hindrance can make immobilized probes inaccessible to their binding partner targets. Small peptides such as oxidized glutathione (GSSG) have been shown to have anti-fouling properties just as effective as BSA, but without introducing steric hindrance—yielding lower detection limits because of greater biorecognition efficacy. [175] However, it may also be due to lower Debye lengths created by an anti-fouling layer closer to the sensing surface.

Unpublished data from our research group shows oxidation of tyrosine amino acids potentially creating a crosslinked monolayer through free radical formation and subsequent polymerization. This crosslinked monolayer can be used as an anti-fouling layer resistant to the Vroman effect whereby smaller proteins are displaced by larger ones, and also resilient to desorption due to its interconnectedness. Since the graphene surface is functionalized using weak bonding forces, it is important to consider potential peptide desorption since loss of anti-fouling regions can expose sensing areas to non-specific adsorption of biological contaminants—creating erroneous sensor readings. Pursuing this tyrosine polymerization approach can reveal additional insight and improvement into peptide-based surface functionalization for biosensing applications.

9.2. Addressing Task 2: Graphene FET Devices

The subtasks associated with Task is underway and has yielded a working testbed for detecting nucleic acid targets.

9.2.1. Characterizing biosensor device performance.

Additional activities include characterizing device performance and detection of biomarkers in synthetic biological fluids. Metrics for determining performance parameters include generating I-V curve response data. Likewise, to ensure selective hybridization with nucleic acids targets, probes that meet criteria for high selectivity (e.g., antisense sequences predicted to be non-promiscuous) will be used. Dysregulated target miRNAs in pancreatic cancer will be screened for low consensus sequences. Probes will be further validated using target sequences containing point mutations[82] to determine specificity and selectivity, ruling out any probes that fail to meet high stringency.

9.2.2. Detection of nucleic acid targets in physiologically-relevant media.

Following detection of nucleic acid targets in biologically osmotic and pH-balanced buffers, simulated physiological media will be replicated and used for biosensing. For example, blood plasma can be replicated by supplementing 1X PBS with BSA. Additionally, native serum samples lacking detectable amounts of the target biomolecule can be spiked with the target biomolecule to serve as a positive sample. Optimizing biosensor performance under these conditions will advance the project closer to its ultimate goal of detecting biomarkers directly from patient samples.

9.2.3. Minimizing the Debye screening for enhanced sensitivity.

The Debye length is the maximum distance beyond which an electric charge can no longer exert influence or effect. This has great relevance to FET-based biosensors because the sensing principle is based on the bound biomolecule perturbing the sensing channel in order to elicit a change in current and yield an electronic sensor signal response. Thus, charge screening by ions in solution can greatly diminish sensor sensitivity and poses a major challenge when detecting molecules in high ionic strength solutions

such as biological fluids and buffers. Being able to increase the Debye length will ultimately strengthen the electrostatic influence of the bound biomolecule on the sensing material.

There are several options[176] available for minimizing the Debye screening: 1) decreasing the ionic strength of the solution; 2) minimizing the distance between the site of probe-target interaction and the sensor surface; 3) introducing a high field-effect through an additional gate; 4) disrupting the electric double layer formed by ions at the solution-surface interface. The objective for each of these strategies is to decrease the charge screening effect imposed by the ions in solution.

The effect of charge screening by high ionic strength solutions can also be mitigated by inducing a field-effect through a gate electrode very close to the transistor channel, thereby creating a solution potential across the gate electrode and the transistor channel.[176] This high-field modulates the channel conductivity and therefor can result in a measurable current gain. Thus, it is possible to re-design the graphene biosensor to accommodate a gate electrode with a high field-effect.

9.2.4. Breaking up the electric double layer.

The presence of an electric double layer (EDL) can diminish FET biosensor sensitivity. This is because charged ions in solution accumulate at the solution-substrate interface and can charge screen the sensing material from the electrostatic effects of the bound target molecule. The formation of an EDL is similar to decreasing the Debye length of the sensing channel rendering it less sensitive to the biomarker target. Thus, minimizing the EDL can extend the effective boundary of the Debye length, which would impart greater detection sensitivity by allowing the sensing material to be less shielded and more easily perturbed by the biorecognition event.[176] Furthermore, incorporating high frequency modulation into the biosensing strategy using alternating current (AC) can break up the electric double layer by removing ions localized at the solution-substrate interface.

Thus, FET-based biosensors using AC-driven signals across the conducting channel can detect protein targets with greater sensitivity in high ionic strength solutions, such as in physiological buffers.[177,178] Since nucleic acids are highly charged molecules that are prone to ionic shielding, the

practicality of applying similar sensing strategies towards nucleic acid detection is reasonable. For example, rather than detecting the change in conductance of the sensing material in a FET device, incorporating high frequency AC modulation can instead detect the perturbance of molecular dipoles of adsorbed molecules.[179] Such an approach is advantageous since it overcomes challenges created by Debye screening effects that render sensing in physiological buffers ineffective. Electrochemical impedance spectroscopy studies can be performed to investigate these effects.

9.3. Addressing Task 3: Multiplexed Detection of miRNA Targets

The subtasks associated with Task 3 will commence fully upon near completion of device performance characterization as outlined in Task 2. However, the device packaging approach and circuitry currently being designed can start being scaled up from one sensor to multiple sensors. However, candidate miRNA biomarker targets have already been identified from research literature and are deemed suitable for early diagnosis of pancreatic cancer.

9.3.1. Possible use of other 2D materials.

In creating a cancer biomarker biosensor, well-characterized GFET-based devices are developed before potentially exploring additional single layer materials. Established microfabrication techniques[180,181] have been used to create FET devices based on graphene. These can be easily adapted to make FET devices based on other 2D materials. For example, molybdenum disulfide is a semiconducting analogue of graphene[182] and is touted as a highly versatile substrate for various sensing platforms.[183] MoS_2 is attractive due to facile production of high quality crystalline 2D layers via chemical vapor deposition[184] or atomic layer depositione[185] techniques, which are amenable to microfabrication techniques. The advantage MoS_2 has over graphene is its bandgap, which graphene lacks, thereby conferring MoS_2 with a semiconducting nature that helps lower background carrier densities—allowing for enhanced sensitivity with lower leakage current, along with permitting optical sensing platforms. MoS_2-binding peptides have already been developed in our research group and so it is possible to pursue a MoS_2-based device.

10. Milestones

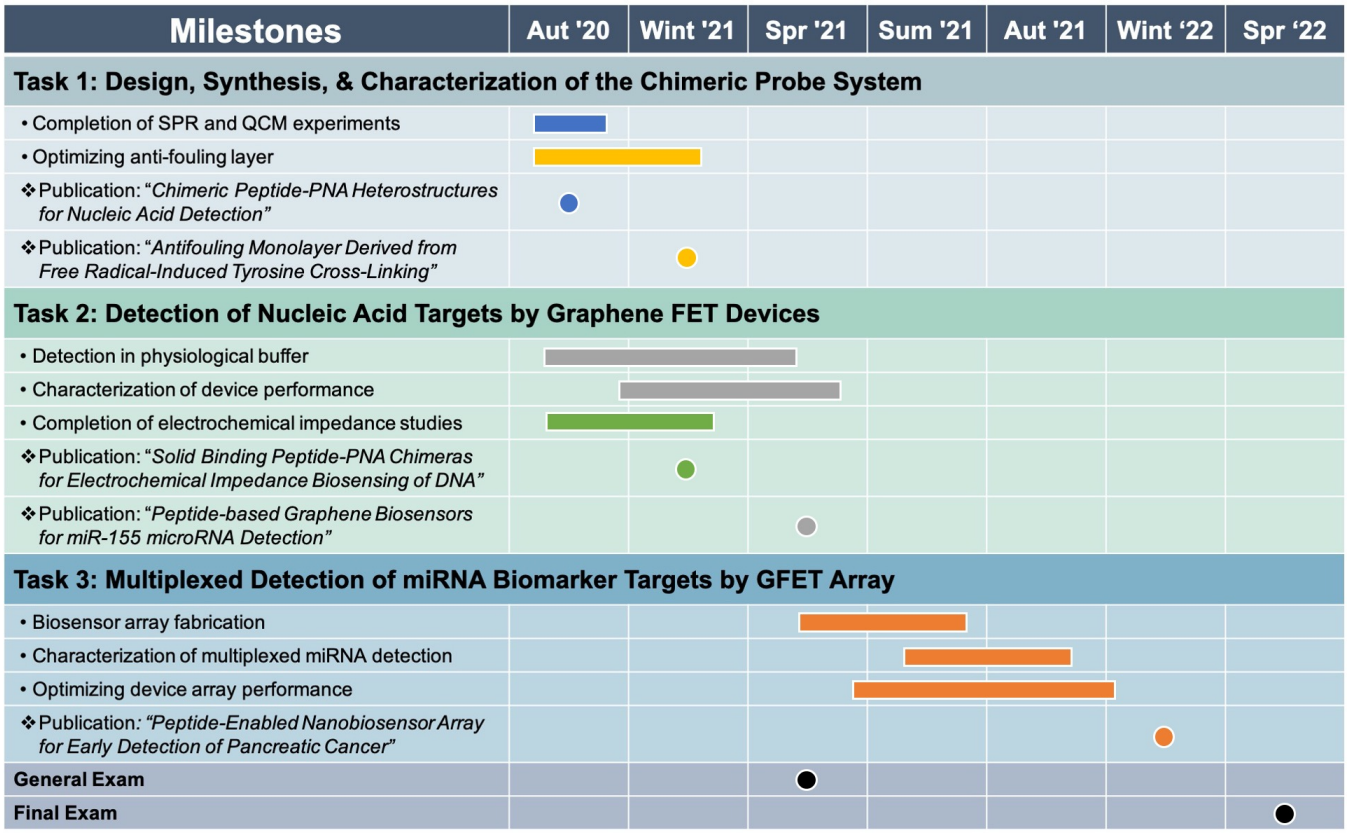

11. Potential Publications

- Chimeric Peptide-PNA Heterostructures for Nucleic Acid Detection
- Solid Binding Peptide-PNA Chimeras for Electrochemical Impedance Biosensing of DNA
- Peptide-based Graphene Biosensors for miR-155 microRNA Detection
- Antifouling Monolayer Derived from Free Radical-Induced Tyrosine Cross-Linking
- Peptide-Enabled Nanobiosensor Array for Early Detection of Pancreatic Cancer

12. Acknowledgements

I would like to thank my graduate advisor and mentor, Prof. Mehmet Sarikaya, whose vision of combining the physical and life sciences has inspired me to pursue novel research at the intersection of biology and materials science. I would also like to thank the following lab members who have provided insight and assistance to this research project: Dr. Hadi Zareie, Dr. Hanson Fong, Dr. Deniz Yucesoy, Dr. Carolyn Gresswell, David Starkebaum, Tyler Jorgenson, Siddharth Rath, and my undergraduate

researchers. This research was supported by the National Science Foundation (NSF) under the Division of Materials Research for the "Designing Materials to Revolutionize and Engineer our Future" (DMREF) program (grant DMR-1629071) as part of the Materials Genome Initiative (MGI), and also by the generous funding from the Amazon Catalyst program through CoMotion at the University of Washington.

13. References

1. Kojima, M. *et al.* MicroRNA markers for the diagnosis of pancreatic and biliary-tract cancers. *PLoS ONE* **10,** e0118220 (2015).
2. Machida, T. *et al.* miR-1246 and miR-4644 in salivary exosome as potential biomarkers for pancreatobiliary tract cancer. *Oncol. Rep.* **36,** 2375–2381 (2016).
3. Liu, R. *et al.* Serum microRNA expression profile as a biomarker in the diagnosis and prognosis of pancreatic cancer. *Clin. Chem.* **58,** 610–618 (2012).
4. Li, A. *et al.* MicroRNA array analysis finds elevated serum miR-1290 accurately distinguishes patients with low-stage pancreatic cancer from healthy and disease controls. *Clinical Cancer Research* **19,** 3600–3610 (2013).
5. Debernardi, S. *et al.* Noninvasive urinary miRNA biomarkers for early detection of pancreatic adenocarcinoma. *Am J Cancer Res* **5,** 3455–3466 (2015).
6. Siegel, R. L., Miller, K. D. & Jemal, A. Cancer statistics, 2016. *CA: A Cancer Journal for Clinicians* **66,** 7–30 (2016).
7. Rahib, L. *et al.* Projecting Cancer Incidence and Deaths to 2030: The Unexpected Burden of Thyroid, Liver, and Pancreas Cancers in the United States. *Cancer Research* **74,** 2913–2921 (2014).
8. Homma, T. & Tsuchiya, R. The study of the mass screening of persons without symptoms and of the screening of outpatients with gastrointestinal complaints or icterus for pancreatic cancer in Japan, using CA19-9 and elastase-1 or ultrasonography. *Int. J. Pancreatol.* **9,** 119–124 (1991).
9. O'Neill, C. B. *et al.* Costs and trends in pancreatic cancer treatment. - PubMed - NCBI. *Cancer* **118,** 5132–5139 (2012).
10. Schultz, N. A. *et al.* MicroRNA Biomarkers in Whole Blood for Detection of Pancreatic Cancer. *JAMA* **311,** 392–404 (2014).
11. Wang, J. *et al.* MicroRNAs in plasma of pancreatic ductal adenocarcinoma patients as novel blood-based biomarkers of disease. *Cancer Prev Res (Phila)* **2,** 807–813 (2009).
12. Hansen, T. B., Kjems, J. & Damgaard, C. K. Circular RNA and miR-7 in Cancer. *Cancer Research* **73,** 5609–5612 (2013).
13. Arnaiz, E. *et al.* CircRNAs and cancer: Biomarkers and master regulators. *Semin. Cancer Biol.* **58,** 90–99 (2019).
14. Kulcheski, F. R., Christoff, A. P. & Margis, R. Circular RNAs are miRNA sponges and can be used as a new class of biomarker. *Journal of Biotechnology* **238,** 42–51 (2016).
15. Zhang, Y. *et al.* Circular RNAs: emerging cancer biomarkers and targets. *J Exp Clin Cancer Res* **36,** 1–13 (2017).
16. Kohler, C., Barekati, Z., Radpour, R. & Zhong, X. Y. Cell-free DNA in the circulation as a potential cancer biomarker. *Anticancer Research* **31,** 2623–2628 (2011).
17. Campos-Carrillo, A. *et al.* Circulating tumor DNA as an early cancer detection tool. *Pharmacol. Ther.* 107458 (2019). doi:10.1016/j.pharmthera.2019.107458

18. Vinny Negi, S. Y. C. Discerning functional hierarchies of microRNAs in pulmonary hypertension. *JCI Insight* **2,** D34 (2017).
19. He, L. & Hannon, G. J. MicroRNAs: small RNAs with a big role in gene regulation. *Nat. Rev. Genet.* **5,** 522–531 (2004).
20. Ha, M. & Kim, V. N. Regulation of microRNA biogenesis. *Nature Reviews Molecular Cell Biology* **15,** 509–524 (2014).
21. Ha, T.-Y. MicroRNAs in Human Diseases: From Cancer to Cardiovascular Disease. *Immune Network* **11,** 135–154 (2011).
22. Jansson, M. D. & Lund, A. H. MicroRNA and cancer. *Molecular Oncology* **6,** 590–610 (2012).
23. Hayes, J., Peruzzi, P. P. & Lawler, S. MicroRNAs in cancer: biomarkers, functions and therapy. *Trends in Molecular Medicine* **20,** 460–469 (2014).
24. Roberts, A. P. E., Lewis, A. P. & Jopling, C. L. The role of microRNAs in viral infection. *Prog Mol Biol Transl Sci* **102,** 101–139 (2011).
25. Powdrill, M. H., Desrochers, G. F., Singaravelu, R. & Pezacki, J. P. The role of microRNAs in metabolic interactions between viruses and their hosts. *Curr Opin Virol* **19,** 71–76 (2016).
26. Romaine, S. P. R., Tomaszewski, M., Condorelli, G. & Samani, N. J. MicroRNAs in cardiovascular disease: an introduction for clinicians. *Heart* **101,** 921–928 (2015).
27. Small, E. M., Frost, R. J. A. & Olson, E. N. MicroRNAs Add a New Dimension to Cardiovascular Disease. *Circulation* **121,** 1022–1032 (2010).
28. Vijayan, M. & Reddy, P. H. Peripheral biomarkers of stroke: Focus on circulatory microRNAs. *Biochimica et Biophysica Acta (BBA) - Molecular Basis of Disease* **1862,** 1984–1993 (2016).
29. Simats, A., García-Berrocoso, T. & Montaner, J. Neuroinflammatory biomarkers: From stroke diagnosis and prognosis to therapy. *Biochimica et Biophysica Acta (BBA) - Molecular Basis of Disease* **1862,** 411–424 (2016).
30. Kye, M. J. & Gonçalves, I. D. C. G. The role of miRNA in motor neuron disease. *Frontiers in Cellular Neuroscience* **8,** (2014).
31. Wang, W., Kwon, E. J. & Tsai, L.-H. MicroRNAs in learning, memory, and neurological diseases. *Learn. Mem.* **19,** 359–368 (2012).
32. Larrea, E. *et al.* New Concepts in Cancer Biomarkers: Circulating miRNAs in Liquid Biopsies. *IJMS* **17,** 627 (2016).
33. Drakaki, A. & Iliopoulos, D. MicroRNA-gene signaling pathways in pancreatic cancer. *Biomedical Journal* **36,** 200–208 (2013).
34. Lee, E. J. *et al.* Expression profiling identifies microRNA signature in pancreatic cancer. *Int. J. Cancer* **120,** 1046–1054 (2007).
35. Schmidt, M. F. Drug target miRNAs: chances and challenges. *Trends in Biotechnology* **32,** 578–585 (2014).
36. Heneghan, H. M., Miller, N. & Kerin, M. J. MiRNAs as biomarkers and therapeutic targets in cancer☆. **10,** 543–550 (2010).
37. Ghai, V. & Wang, K. Recent progress toward the use of circulating microRNAs as clinical biomarkers. *Arch. Toxicol.* 1–20 (2016). doi:10.1007/s00204-016-1828-2
38. Gayral, M. *et al.* MicroRNAs as emerging biomarkers and therapeutic targets for pancreatic cancer. *World J. Gastroenterol.* **20,** 11199–11209 (2014).
39. Li, Y. & Sarkar, F. H. MicroRNA Targeted Therapeutic Approach for Pancreatic Cancer. *International Journal of Biological Sciences* **12,** 326–337 (2016).
40. Humeau, M., Torrisani, J. & Cordelier, P. miRNA in clinical practice: pancreatic cancer. *Clin. Biochem.* **46,** 933–936 (2013).

41. Mitchell, P. S. *et al.* Circulating microRNAs as stable blood-based markers for cancer detection. *Proc. Natl. Acad. Sci. U.S.A.* **105,** 10513–10518 (2008).
42. Mall, C., Rocke, D. M., Durbin-Johnson, B. & Weiss, R. H. Stability of miRNA in human urine supports its biomarker potential. *Biomark Med* **7,** 623–631 (2013).
43. Gilad, S. *et al.* Serum MicroRNAs Are Promising Novel Biomarkers. *PLoS ONE* **3,** e3148 (2008).
44. Tavallaie, R., De Almeida, S. R. M. & Gooding, J. J. Toward biosensors for the detection of circulating microRNA as a cancer biomarker: an overview of the challenges and successes. *Wiley Interdisciplinary Reviews: Nanomedicine and Nanobiotechnology* **7,** 580–592 (2015).
45. Dong, H. *et al.* MicroRNA: function, detection, and bioanalysis. *Chemical Reviews* **113,** 6207–6233 (2013).
46. Torsi, L., Magliulo, M., Manoli, K. & Palazzo, G. Organic field-effect transistor sensors: a tutorial review. *Chem Soc Rev* **42,** 8612–8628 (2013).
47. Johnson, B. N. & Mutharasan, R. Biosensor-based microRNA detection: techniques, design, performance, and challenges. *Analyst* **139,** 1576–1588 (2014).
48. Veigas, B., Fortunato, E. & Baptista, P. V. Field effect sensors for nucleic Acid detection: recent advances and future perspectives. *Sensors (Basel)* **15,** 10380–10398 (2015).
49. Labib, M. & Berezovski, M. V. Electrochemical sensing of microRNAs: avenues and paradigms. *Biosensors and Bioelectronics* **68,** 83–94 (2015).
50. Johnson, B. N. & Mutharasan, R. Sample preparation-free, real-time detection of microRNA in human serum using piezoelectric cantilever biosensors at attomole level. *Analytical Chemistry* **84,** 10426–10436 (2012).
51. Wu, P., Tu, Y., Qian, Y., Zhang, H. & Cai, C. DNA strand-displacement-induced fluorescence enhancement for highly sensitive and selective assay of multiple microRNA in cancer cells. *Chem. Commun. (Camb.)* **50,** 1012–1014 (2013).
52. Su, S. *et al.* DNA-conjugated quantum dot nanoprobe for high-sensitivity fluorescent detection of DNA and micro-RNA. *ACS Appl Mater Interfaces* **6,** 1152–1157 (2014).
53. Syu, Y. C., Hsu, W. E. & Lin, C. T. Review-field-effect transistor biosensing: Devices and clinical applications. *ECS J. Solid State Sci. Technol.* **7,** Q3196–Q3207 (2018).
54. Kaisti, M. Detection principles of biological and chemical FET sensors. *Biosensors and Bioelectronics* **98,** 437–448 (2017).
55. Park, J., Nguyen, H. H., Woubit, A. & Kim, M. Applications of Field-Effect Transistor (FET)-Type Biosensors. *Applied Science and …* (2014).
56. Lee, J. *et al.* Two-dimensional layered MoS2 biosensors enable highly sensitive detection of biomolecules. **4,** 7352 (2014).
57. Mohanty, N. & Berry, V. Graphene-Based Single-Bacterium Resolution Biodevice and DNA Transistor: Interfacing Graphene Derivatives with Nanoscale and Microscale Biocomponents. **8,** 4469–4476 (2008).
58. Novoselov, K. S. Electric Field Effect in Atomically Thin Carbon Films. *Science* **306,** 666–669 (2004).
59. Geim, A. K. & Novoselov, K. S. The rise of graphene. *Nature Materials* **6,** 183–191 (2007).
60. Zhu, Y. *et al.* Graphene and Graphene Oxide: Synthesis, Properties, and Applications. *Adv. Mater.* **22,** 3906–3924 (2010).
61. Liu, Y., Dong, X. & Chen, P. Biological and chemical sensors based on graphene materials. *Chem Soc Rev* **41,** 2283–2307 (2012).
62. Shan, C. *et al.* Direct Electrochemistry of Glucose Oxidase and Biosensing for Glucose Based on Graphene. *Analytical Chemistry* **81,** 2378–2382 (2009).
63. Zhu, C. & Dong, S. Energetic Graphene-Based Electrochemical Analytical Devices in

Nucleic Acid, Protein and Cancer Diagnostics and Detection. *Electroanalysis* **26,** 14–29 (2013).
64. Lin, Y. M. *et al.* Wafer-Scale Graphene Integrated Circuit. *Science* **332,** 1294–1297 (2011).
65. Wang, H. *et al.* Integrated Circuits Based on Bilayer MoS 2Transistors. *Nano Lett.* **12,** 4674–4680 (2012).
66. Radisavljevic, B., Radenovic, A., Brivio, J., Giacometti, V. & Kis, A. Single-layer MoS2 transistors. *Nature Nanotechnology* **6,** 147–150 (2011).
67. Sarikaya, M., Tamerler, C., Jen, A. K. Y., Schulten, K. & Baneyx, F. Molecular biomimetics: nanotechnology through biology. *Nature Materials* **2,** 577–585 (2003).
68. Care, A., Bergquist, P. L. & Sunna, A. Solid-binding peptides: smart tools for nanobiotechnology. *Trends in Biotechnology* **33,** 259–268 (2015).
69. Donatan, S., Sarikaya, M., Tamerler, C. & Urgen, M. Effect of solid surface charge on the binding behaviour of a metal-binding peptide. *J R Soc Interface* **9,** 2688–2695 (2012).
70. Hayamizu, Y. *et al.* Bioelectronic interfaces by spontaneously organized peptides on 2D atomic single layer materials. *Scientific Reports* **6,** 33778 (2016).
71. Kacar, T. *et al.* Quartz Binding Peptides as Molecular Linkers towards Fabricating Multifunctional Micropatterned Substrates. *Adv. Mater. Weinheim* **21,** 295–299 (2009).
72. Hnilova, M. *et al.* Single-step fabrication of patterned gold film array by an engineered multi-functional peptide. *Journal of Colloid and Interface Science* **365,** 97–102 (2012).
73. Tamerler, C. *et al.* Materials Specificity and Directed Assembly of a Gold-Binding Peptide. **2,** 1372–1378 (2006).
74. So, C. R., Tamerler, C. & Sarikaya, M. Adsorption, Diffusion, and Self-Assembly of an Engineered Gold-Binding Peptide on Au(111) Investigated by Atomic Force Microscopy. *Angewandte Chemie* **121,** 5276–5279 (2009).
75. Khatayevich, D. *et al.* Biofunctionalization of materials for implants using engineered peptides. *Acta Biomaterialia* **6,** 4634–4641 (2010).
76. Khatayevich, D. *et al.* Selective detection of target proteins by peptide-enabled graphene biosensor. *Small* **10,** 1505–1513 (2014).
77. Wang, J. DNA biosensors based on Peptide Nucleic Acid (PNA) recognition layers. A review1This paper was a finalist for the Biosensors & Bioelectronics Award for the most original contribution to the Congress.1. *Biosensors and Bioelectronics* **13,** 757–762 (1998).
78. Shakeel, S., Karim, S. & Ali, A. Peptide nucleic acid (PNA) — a review. *Journal of Chemical Technology and Biotechnology* **81,** 892–899 (2006).
79. Siddiquee, S. A Review of Peptide Nucleic Acid. *Advanced Techniques in Biology & Medicine* **03,** (2015).
80. Egholm, M. *et al.* PNA hybridizes to complementary oligonucleotides obeying the Watson–Crick hydrogen-bonding rules. *Nature Nanotechnology* **365,** 566–568 (1993).
81. Chakrabarti, M. C. & Schwarz, F. P. Thermal stability of PNA/DNA and DNA/DNA duplexes by differential scanning calorimetry. *Nucleic Acids Research* **27,** 4801–4806 (1999).
82. Igloi, G. L. Variability in the stability of DNA-peptide nucleic acid (PNA) single-base mismatched duplexes: Real-time hybridization during affinity electrophoresis in PNA-containing gels. *Proceedings of the National Academy of Sciences* **95,** 8562–8567 (1998).
83. Ratilainen, T., Holmén, A., Tuite, E., Nielsen, P. E. & Norden, B. Thermodynamics of Sequence-Specific Binding of PNA to DNA †. *Biochemistry* **39,** 7781–7791 (2000).
84. Karkare, S. & Bhatnagar, D. Promising nucleic acid analogs and mimics: characteristic features and applications of PNA, LNA, and morpholino. *Appl. Microbiol. Biotechnol.* **71,** 575–586 (2006).
85. Zu, Y., Ting, A. L., Yi, G. & Gao, Z. Sequence-Selective Recognition of Nucleic Acids

under Extremely Low Salt Conditions Using Nanoparticle Probes. *Analytical Chemistry* **83,** 4090–4094 (2011).
86. Wang, G. & Xu, X. S. Peptide nucleic acid (PNA) binding-mediated gene regulation. *Cell Research* **14,** 111–116 (2004).
87. Wu, G., Tang, X., Meyyappan, M. & Lai, K. W. C. Doping effects of surface functionalization on graphene with aromatic molecule and organic solvents. *Applied Surface Science* **425,** 713–721 (2017).
88. So, C. R. *et al.* Controlling Self-Assembly of Engineered Peptides on Graphite by Rational Mutation. *ACS Nano* **6,** 1648–1656 (2012).
89. Schmidt, C. Early detection tools for pancreatic cancer. *Journal of the National Cancer Institute* **104,** 1117–1118 (2012).
90. Mccarthy, Evans, SagarNeoptolemos. Prediction of resectability of pancreatic malignancy by computed tomography. *British Journal of Surgery* **85,** 320–325 (1998).
91. Rösch, T. *et al.* Localization of Pancreatic Endocrine Tumors by Endoscopic Ultrasonography. *N Engl J Med* **326,** 1721–1726 (1992).
92. Verna, E. C. *et al.* Pancreatic cancer screening in a prospective cohort of high-risk patients: a comprehensive strategy of imaging and genetics. *Clinical Cancer Research* **16,** 5028–5037 (2010).
93. Zubarik, R. *et al.* Screening for pancreatic cancer in a high-risk population with serum CA 19-9 and targeted EUS: a feasibility study. *Gastrointestinal Endoscopy* **74,** 87–95 (2011).
94. Seufferlein, T., Bachet, J. B., Van Cutsem, E., Rougier, P.ESMO Guidelines Working Group. Pancreatic adenocarcinoma: ESMO-ESDO Clinical Practice Guidelines for diagnosis, treatment and follow-up. **23 Suppl 7,** vii33–40 (2012).
95. Magnani, J. L., Steplewski, Z., Koprowski, H. & Ginsburg, V. Identification of the gastrointestinal and pancreatic cancer-associated antigen detected by monoclonal antibody 19-9 in the sera of patients as a mucin. *Cancer Research* **43,** 5489–5492 (1983).
96. Haglund, C., Lindgren, J., Roberts, P. J. & Nordling, S. Gastrointestinal cancer-associated antigen CA 19-9 in histological specimens of pancreatic tumours and pancreatitis. *British Journal of Cancer* **53,** 189–195 (1986).
97. Martin, L. K., Wei, L., Trolli, E. & Bekaii-Saab, T. Elevated baseline CA19-9 levels correlate with adverse prognosis in patients with early- or advanced-stage pancreas cancer. *Med Oncol* **29,** 3101–3107 (2012).
98. Pleskow, D. K. *et al.* Evaluation of a Serologic Marker, CA19-9, in the Diagnosis of Pancreatic Cancer. *Ann Intern Med* **110,** 704–709 (1989).
99. Winter, J. M., Yeo, C. J. & Brody, J. R. Diagnostic, prognostic, and predictive biomarkers in pancreatic cancer. *Journal of Surgical Oncology* **107,** 15–22 (2013).
100. Ritchie, S. A. *et al.* Pancreatic cancer serum biomarker PC-594: Diagnostic performance and comparison to CA19-9. *World J. Gastroenterol.* **21,** 6604–6612 (2015).
101. Frebourg, T. *et al.* The evaluation of CA 19-9 antigen level in the early detection of pancreatic cancer: A prospective study of 866 patients. *Cancer* **62,** 2287–2290 (1988).
102. Goonetilleke, K. S. & Siriwardena, A. K. Systematic review of carbohydrate antigen (CA 19-9) as a biochemical marker in the diagnosis of pancreatic cancer. - PubMed - NCBI. *European Journal of Surgical Oncology (EJSO)* **33,** 266–270 (2007).
103. Onal, C., Colakoglu, T., Ulusan, S. N., Yapar, A. F. & Kayaselcuk, F. Binary Obstruction Induces Extremely Elevated Serum CA 19-9 Levels: Case Report. *Onkologie* **35,** 780–782 (2012).
104. Tempero, M. A. *et al.* Relationship of carbohydrate antigen 19-9 and Lewis antigens in pancreatic cancer. *Cancer Research* **47,** 5501–5503 (1987).
105. KIM, J.-E. *et al.* Clinical usefulness of carbohydrate antigen 19-9 as a screening test for

pancreatic cancer in an asymptomatic population. *J. Gastroenterol. Hepatol.* **19,** 182–186 (2004).
106. Satake, K., Takeuchi, T., Homma, T. & Ozaki, H. CA19-9 as a Screening and Diagnostic Tool in Symptomatic Patients. *Pancreas* **9,** 703–706 (1994).
107. Ritchie, S. A. *et al.* Metabolic system alterations in pancreatic cancer patient serum: potential for early detection. *BMC Cancer* **13,** (2013).
108. Jia Zhao *et al.* Glycoprotein Microarrays with Multi-Lectin Detection: Unique Lectin Binding Patterns as a Tool for Classifying Normal, Chronic Pancreatitis and Pancreatic Cancer Sera. *Journal of proteome …* **6,** 1864–1874 (2007).
109. Nie, S. *et al.* Glycoprotein Biomarker Panel for Pancreatic Cancer Discovered by Quantitative Proteomics Analysis. *J. Proteome Res.* **13,** 1873–1884 (2014).
110. Kenner, B. J. *et al.* Early Detection of Pancreatic Cancer-a Defined Future Using Lessons From Other Cancers: A White Paper. *Pancreas* **45,** 1073–1079 (2016).
111. Tian, T., Wang, J. & Zhou, X. A review: microRNA detection methods. *Org. Biomol. Chem.* **13,** 2226–2238 (2015).
112. Pritchard, C. C., Cheng, H. H. & Tewari, M. MicroRNA profiling: approaches and considerations. *Nat. Rev. Genet.* **13,** 358–369 (2012).
113. Chen, C. *et al.* Real-time quantification of microRNAs by stem-loop RT-PCR. *Nucleic Acids Research* **33,** e179–e179 (2005).
114. Davison, T. S., Johnson, C. D. & Andruss, B. F. Analyzing micro-RNA expression using microarrays. *Meth. Enzymol.* **411,** 14–34 (2006).
115. Liu, C.-G., Spizzo, R., Calin, G. A. & Croce, C. M. Expression profiling of microRNA using oligo DNA arrays. *Methods* **44,** 22–30 (2008).
116. Yin, J. Q., Zhao, R. C. & Morris, K. V. Profiling microRNA expression with microarrays. *Trends in Biotechnology* **26,** 70–76 (2008).
117. Bargaje, R., Hariharan, M., Scaria, V. & Pillai, B. Consensus miRNA expression profiles derived from interplatform normalization of microarray data. *RNA* **16,** 16–25 (2010).
118. Müller, S. *et al.* Next-generation sequencing reveals novel differentially regulated mRNAs, lncRNAs, miRNAs, sdRNAs and a piRNA in pancreatic cancer. *Molecular Cancer* **14,** 607 (2015).
119. Lee, L. W. *et al.* Complexity of the microRNA repertoire revealed by next-generation sequencing. *RNA* **16,** 2170–2180 (2010).
120. Koshiol, J., Wang, E., Zhao, Y., Marincola, F. & Landi, M. T. Strengths and limitations of laboratory procedures for microRNA detection. *Cancer Epidemiol. Biomarkers Prev.* **19,** 907–911 (2010).
121. Bearden, E. D., Simpson, P. M., Peterson, C. A. & Beggs, M. L. Assessing the Reliability of Amplified RNA Used in Microarrays. *Applied Bioinformatics* **5,** 67–76 (2006).
122. Chen, Y., Gelfond, J. A., McManus, L. M. & Shireman, P. K. Reproducibility of quantitative RT-PCR array in miRNA expression profiling and comparison with microarray analysis. *BMC Genomics* **10,** 407 (2009).
123. Hnilova, M. *et al.* Effect of molecular conformations on the adsorption behavior of gold-binding peptides. *Langmuir* **24,** 12440–12445 (2008).
124. Gong, P., Lee, C.-Y., Gamble, L. J., Castner, D. G. & Grainger, D. W. Hybridization Behavior of Mixed DNA/Alkylthiol Monolayers on Gold: Characterization by Surface Plasmon Resonance and 32P Radiometric Assay. *Analytical Chemistry* **78,** 3326–3334 (2006).
125. Jung, L. S., Campbell, C. T., Chinowsky, T. M., Mar, M. N. & Yee, S. S. Quantitative Interpretation of the Response of Surface Plasmon Resonance Sensors to Adsorbed Films. *Langmuir* **14,** 5636–5648 (1998).

126. Peterson, A. W. & Heaton, R. J. The effect of surface probe density on DNA hybridization. *Nucleic Acids Research* **29,** 5163–5168 (2001).
127. Xu, F., Pellino, A. M. & Knoll, W. Electrostatic repulsion and steric hindrance effects of surface probe density on deoxyribonucleic acid (DNA)/peptide nucleic acid (PNA) hybridization. *Thin Solid Films* **516,** 8634–8639 (2008).
128. Schmidt, C. Urine biomarkers may someday detect even distant tumors. *Journal of the National Cancer Institute* **101,** 8–10 (2009).
129. Mengual, L. *et al.* Using microRNA profiling in urine samples to develop a non-invasive test for bladder cancer. *Int. J. Cancer* **133,** 2631–2641 (2013).
130. Cote, G. A. *et al.* A Pilot Study to Develop a Diagnostic Test for Pancreatic Ductal Adenocarcinoma Based on Differential Expression of Select miRNA in Plasma and Bile. *The American Journal of Gastroenterology* **109,** 1942–1952 (2014).
131. Hernandez, Y. G. & Lucas, A. L. MicroRNA in pancreatic ductal adenocarcinoma and its precursor lesions. *World J Gastrointest Oncol* **8,** 18–29 (2016).
132. Wentz, S. C. & Shi, C. *Pancreatic Cancer and Its Precursor Lesions*. *Pathobiology of Human Disease A Dynamic Encyclopedia of Disease Mechanisms* 2251–2264 (2014). doi:10.1016/B978-0-12-386456-7.04904-2
133. Yu, J., Li, A., Hong, S.-M., Hruban, R. H. & Goggins, M. MicroRNA Alterations of Pancreatic Intraepithelial Neoplasms (PanINs). *Clinical Cancer Research* **18,** 981–992 (2012).
134. Lee, L. S. *et al.* Investigating MicroRNA Expression Profiles in Pancreatic Cystic Neoplasms. *Clinical and Translational Gastroenterology* **5,** e47 (2014).
135. Vila-Navarro, E. *et al.* MicroRNAs for Detection of Pancreatic Neoplasia: Biomarker Discovery by Next-generation Sequencing and Validation in 2 Independent Cohorts. *Ann. Surg.* **265,** 1226–1234 (2017).
136. Alemar, B., Gregório, C. & Ashton-Prolla, P. miRNAs As Diagnostic and Prognostic Biomarkers in Pancreatic Ductal Adenocarcinoma and Its Precursor Lesions: A Review. *Biomark Insights* **10,** 113–124 (2015).
137. Habbe, N. *et al.* MicroRNA miR-155 is a biomarker of early pancreatic neoplasia. *Cancer Biology & Therapy* **8,** 340–346 (2014).
138. Ali, S., Almhanna, K., Chen, W., Philip, P. A. & Sarkar, F. H. Differentially expressed miRNAs in the plasma may provide a molecular signature for aggressive pancreatic cancer. *Am J Transl Res* **3,** 28–47 (2011).
139. Pei, Z. *et al.* Clinically relevant circulating microRNA profiling studies in pancreatic cancer using meta-analysis. *Oncotarget* **8,** 22616–22624 (2017).
140. Arroyo, J. D. *et al.* Argonaute2 complexes carry a population of circulating microRNAs independent of vesicles in human plasma. *Proc. Natl. Acad. Sci. U.S.A.* **108,** 5003–5008 (2011).
141. Wang, K., Zhang, S., Weber, J., Baxter, D. & Galas, D. J. Export of microRNAs and microRNA-protective protein by mammalian cells. *Nucleic Acids Research* **38,** 7248–7259 (2010).
142. Turchinovich, A., Weiz, L., Langheinz, A. & Burwinkel, B. Characterization of extracellular circulating microRNA. **39,** 7223–7233 (2011).
143. Hunter, M. P. *et al.* Detection of microRNA expression in human peripheral blood microvesicles. *PLoS ONE* **3,** e3694 (2008).
144. Valadi, H. *et al.* Exosome-mediated transfer of mRNAs and microRNAs is a novel mechanism of genetic exchange between cells. *Nature Cell Biology* **9,** 654–659 (2007).
145. Simons, M. & Raposo, G. Exosomes--vesicular carriers for intercellular communication. *Curr. Opin. Cell Biol.* **21,** 575–581 (2009).

146. Théry, C., Zitvogel, L. & Amigorena, S. Exosomes: composition, biogenesis and function. *Nature Reviews Immunology* **2,** 569–579 (2002).
147. Chevillet, J. R. *et al.* Quantitative and stoichiometric analysis of the microRNA content of exosomes. *Proc. Natl. Acad. Sci. U.S.A.* **111,** 14888–14893 (2014).
148. Dame, G., Lampe, J., Hakenberg, S. & Urban, G. Development of a Fast miRNA Extraction System for Tumor Analysis Based on a Simple Lab on Chip Approach. *Procedia Engineering* **120,** 158–162 (2015).
149. Herne, T. M. & Tarlov, M. J. Characterization of DNA Probes Immobilized on Gold Surfaces. *Journal of the American Chemical Society* **119,** 8916–8920 (1997).
150. Lee, C.-Y. *et al.* Surface coverage and structure of mixed DNA/alkylthiol monolayers on gold: characterization by XPS, NEXAFS, and fluorescence intensity measurements. *Analytical Chemistry* **78,** 3316–3325 (2006).
151. Xu, S. *et al.* Real-time reliable determination of binding kinetics of DNA hybridization using a multi-channel graphene biosensor. *Nat Commun* **8,** 14902 (2017).
152. Molitor, F. *et al.* Local gating of a graphene Hall bar by graphene side gates. *Physical Review B* **76,** 245426 (2007).
153. Abergel, D. S. L., Russell, A. & Fal'ko, V. I. Visibility of graphene flakes on a dielectric substrate. *Applied Physics Letters* **91,** 063125 (2007).
154. Bauer, A. S. *et al.* Diagnosis of pancreatic ductal adenocarcinoma and chronic pancreatitis by measurement of microRNA abundance in blood and tissue. *PLoS ONE* **7,** e34151 (2012).
155. Li, A. *et al.* Pancreatic cancers epigenetically silence SIP1 and hypomethylate and overexpress miR-200a/200b in association with elevated circulating miR-200a and miR-200b levels. *Cancer Research* **70,** 5226–5237 (2010).
156. Alemar, B. *et al.* miRNA-21 and miRNA-34a Are Potential Minimally Invasive Biomarkers for the Diagnosis of Pancreatic Ductal Adenocarcinoma. *Pancreas* **45,** 84–92 (2016).
157. Morimura, R. *et al.* Novel diagnostic value of circulating miR-18a in plasma of patients with pancreatic cancer. *British Journal of Cancer* **105,** 1733–1740 (2011).
158. Liu, J. *et al.* Combination of plasma microRNAs with serum CA19-9 for early detection of pancreatic cancer. *Int. J. Cancer* **131,** 683–691 (2012).
159. Abue, M. *et al.* Circulating miR-483-3p and miR-21 is highly expressed in plasma of pancreatic cancer. *International Journal of Oncology* **46,** 539–547 (2015).
160. Kawaguchi, T. *et al.* Clinical impact of circulating miR-221 in plasma of patients with pancreatic cancer. *British Journal of Cancer* **108,** 361–369 (2013).
161. Zhou, X. *et al.* Diagnostic value of a plasma microRNA signature in gastric cancer: a microRNA expression analysis. *Scientific Reports* **5,** 11251 (2015).
162. Madden, S. F. *et al.* Detecting microRNA activity from gene expression data. *BMC Bioinformatics 2010 11:1* **11,** 257 (2010).
163. Lu, M. *et al.* An Analysis of Human MicroRNA and Disease Associations. *PLoS ONE* **3,** e3420 (2008).
164. Barrett, T. *et al.* NCBI GEO: archive for high-throughput functional genomic data. *Nucleic Acids Research* **37,** D885–D890 (2009).
165. Barrett, T. *et al.* NCBI GEO: archive for functional genomics data sets--10 years on. *Nucleic Acids Research* **39,** D1005–D1010 (2010).
166. Barrett, T. *et al.* NCBI GEO: archive for functional genomics data sets--update. *Nucleic Acids Research* **41,** D991–D995 (2012).
167. Lu, J. *et al.* MicroRNA expression profiles classify human cancers. *Nature Nanotechnology* **435,** 834–838 (2005).
168. Munding, J. B. *et al.* Global microRNA expression profiling of microdissected tissues identifies miR-135b as a novel biomarker for pancreatic ductal adenocarcinoma. *Int. J.*

Cancer **131,** E86–E95 (2011).
169. Sergeant, G., van Eijsden, R., Roskams, T., Van Duppen, V. & Topal, B. Pancreatic cancer circulating tumour cells express a cell motility gene signature that predicts survival after surgery. *BMC Cancer* **12,** 57 (2012).
170. Badea, L., Herlea, V., Dima, S. O., Dumitrascu, T. & Popescu, I. Combined gene expression analysis of whole-tissue and microdissected pancreatic ductal adenocarcinoma identifies genes specifically overexpressed in tumor epithelia. *Hepatogastroenterology* **55,** 2016–2027 (2008).
171. Pei, H. *et al.* FKBP51 affects cancer cell response to chemotherapy by negatively regulating Akt. - PubMed - NCBI. *Cancer Cell* **16,** 259–266 (2009).
172. Zhang, L. *et al.* Salivary transcriptomic biomarkers for detection of resectable pancreatic cancer. - PubMed - NCBI. *Gastroenterology* **138,** 949–957.e7 (2010).
173. Dominy, B. N., Perl, D., Schmid, F. X. & Brooks, C. L., III. The Effects of Ionic Strength on Protein Stability: The Cold Shock Protein Family. *Journal of Molecular Biology* **319,** 541–554 (2002).
174. Schildkraut, C. & Lifson, S. Dependence of the melting temperature of DNA on salt concentration. *Biopolymers* **3,** 195–208 (1965).
175. Lin, Y., Liu, K., Wang, C., Li, L. & Liu, Y. Electrochemical immunosensor for detection of epidermal growth factor reaching lower detection limit: toward oxidized glutathione as a more efficient blocking reagent for the antibody functionalized silver nanoparticles and antigen interaction. *Analytical Chemistry* **87,** 8047–8051 (2015).
176. Sarangadharan, I. *et al.* Review—High Field Modulated FET Biosensors for Biomedical Applications. *ECS J. Solid State Sci. Technol.* **7,** Q3032–Q3042 (2018).
177. Chu, C.-H. *et al.* Beyond the Debye length in high ionic strength solution: direct protein detection with field-effect transistors (FETs) in human serum. *Scientific Reports* **7,** 131 (2017).
178. Kulkarni, G. S. & Zhong, Z. Detection beyond the Debye Screening Length in a High-Frequency Nanoelectronic Biosensor. *Nano Lett.* **12,** 719–723 (2012).
179. Kulkarni, G. S., Zang, W. & Zhong, Z. Nanoelectronic Heterodyne Sensor: A New Electronic Sensing Paradigm. *Acc. Chem. Res.* **49,** 2578–2586 (2016).
180. Molitor, F. *et al.* Energy and transport gaps in etched graphene nanoribbons. *Semicond. Sci. Technol.* **25,** 034002 (2010).
181. Güttinger, J. *et al.* Transport through graphene quantum dots. *Rep. Prog. Phys.* **75,** 126502 (2012).
182. Xie, L. M. Two-dimensional transition metal dichalcogenide alloys: preparation, characterization and applications. *Nanoscale* **7,** 18392–18401 (2015).
183. Gan, X., Zhao, H. & Quan, X. Two-dimensional MoS2: A promising building block for biosensors. *Biosensors and Bioelectronics* **89,** 56–71 (2017).
184. Shi, Y., Li, H. & Li, L.-J. Recent advances in controlled synthesis of two-dimensional transition metal dichalcogenides via vapour deposition techniques. *Chem Soc Rev* **44,** 2744–2756 (2015).
185. Browning, R. *et al.* Atomic layer deposition of MoS2 thin films. *Mater. Res. Express* **2,** 035006 (2015).